6-2019

Spatial and temporal variability of inherent and apparent optical properties in western Lake Erie: Implications for water quality remote sensing

Michael Sayers
Michigan Technological University, mjsayers@mtu.edu

Karl Bosse
Michigan Technological University, krbosse@mtu.edu

Robert Shuchman
Michigan Technological University, shuchman@mtu.edu

Steven A. Ruberg
National Oceanic and Atmospheric Administration

Gary L. Fahnenstiel
Michigan Technological University, glfahnen@mtu.edu

See next page for additional authors.

Follow this and additional works at: https://digitalcommons.mtu.edu/michigantech-p

Part of the Remote Sensing Commons

Recommended Citation

Sayers, M., Bosse, K., Shuchman, R., Ruberg, S. A., Fahnenstiel, G. L., Leshkevich, G., & et al. (2019). Spatial and temporal variability of inherent and apparent optical properties in western Lake Erie: Implications for water quality remote sensing. *Journal of Great Lakes Research, 45*(3), 490-507. http://doi.org/10.1016/j.jglr.2019.03.011
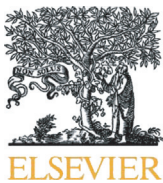Retrieved from: https://digitalcommons.mtu.edu/michigantech-p/634

Follow this and additional works at: https://digitalcommons.mtu.edu/michigantech-p

Part of the Remote Sensing Commons

Authors

Michael Sayers, Karl Bosse, Robert Shuchman, Steven A. Ruberg, Gary L. Fahnenstiel, George Leshkevich, and et al.

Spatial and temporal variability of inherent and apparent optical properties in western Lake Erie: Implications for water quality remote sensing

Michael J. Sayers [a,*], Karl R. Bosse [a], Robert A. Shuchman [a], Steven A. Ruberg [b], Gary L. Fahnenstiel [a], George A. Leshkevich [b], Dack G. Stuart [c], Thomas H. Johengen [c], Ashley M. Burtner [c], Danna Palladino [c]

[a] Michigan Tech Research Institute, Michigan Technological University, 3600 Green Court, Suite 100, Ann Arbor, MI 48105, USA
[b] Great Lakes Environmental Research Laboratory, National Oceanic and Atmospheric Administration, 4840 S. State Road, Ann Arbor, MI 48108, USA
[c] Cooperative Institute for Great Lakes Research (CIGLR), University of Michigan, G110 Dana Building, 440 Church Street, Ann Arbor, MI 48109, USA

ARTICLE INFO

ABSTRACT

Lake Erie has experienced dramatic changes in water quality over the past several decades requiring extensive monitoring to assess effectiveness of adaptive management strategies. Remote sensing offers a unique potential to provide synoptic monitoring at daily time scales complementing in-situ sampling activities occurring in Lake Erie. Bio-optical remote sensing algorithms require knowledge about the inherent optical properties (IOPs) of the water for parameterization to produce robust water quality products. This study reports new IOP and apparent optical property (AOP) datasets for western Lake Erie that encapsulate the May–October period for 2015 and 2016 at weekly sampling intervals. Previously reported IOP and AOP observations have been temporally limited and have not assessed statistical differences between IOPs over spatial and temporal gradients. The objective of this study is to assess trends in IOPs over variable spatial and temporal scales. Large spatio-temporal variability in IOPs was observed between 2015 and 2016 likely due to the difference in the extent and duration of mid-summer cyanobacteria blooms. Differences in the seasonal trends of the specific phytoplankton absorption coefficient between 2015 and 2016 suggest differing algal assemblages between the years. Other IOP variables, including chromophoric, dissolved organic matter (CDOM) and beam attenuation spectral slopes, suggest variability is influenced by river discharge and sediment re-suspension. The datasets presented in this study show how these IOPs and AOPs change over a season and between years, and are useful in advancing the applicability and robustness of remote sensing methods to retrieve water quality information in western Lake Erie.

Introduction and background

Over the past several decades the western basin of Lake Erie has experienced dramatic changes in water quality (Kane et al., 2014) that have negatively impacted the millions of people who rely on the lake for a source of drinking water, a place to recreate, and a location to run their businesses. Of particular concern are the annually recurring blooms of harmful cyanobacteria (cyanoHABs) that occur in the western basin, which in recent years are becoming more persistent and intense (Bridgeman et al., 2013, Michalak et al., 2013, Stumpf et al., 2012, 2016, Sayers et al., 2016, this issue). Annual cyanoHAB occurrences have been linked to the annual spring discharge from the Maumee River (Stumpf et al., 2012, 2016) which provides the large quantities of nutrients required to fuel these blooms. Long-term internal

phosphorus loading of the basin has also recently been shown to play a role in annual cyanoHAB occurrence (Ho and Michalak, 2017). Further complicating our understanding of bloom dynamics, is the abundance of filter feeding dreissenid mussels present in the western basin, which have been linked to increased cyanoHABs through selective feeding and nutrient cycling (Vanderploeg et al., 2001; Conroy et al., 2005; Smith et al., 2015). Fully understanding the combined effect of the many forcing functions on Lake Erie's water quality, more and better water quality measurements will be needed.

Traditional water quality monitoring in Lake Erie has been conducted using in situ and laboratory observations. The USEPA Great Lakes National Program Office (GLNPO) has conducted spring and summer water quality sampling on Lake Erie since the early 1980s (Barbiero et al., 2018) and the NOAA Great Lakes Environmental Research Laboratory (GLERL) has been conducting weekly monitoring for over five years. Many other universities and agencies also have monitoring programs producing valuable data sets. Even with the impressive number

* Corresponding author.
  E-mail address: mjsayers@mtu.edu (M.J. Sayers).

of assets making crucial measurements, it is likely not possible to fully capture the spatial and temporal variability of various water quality parameters in Lake Erie with in situ data alone.

Satellite remote sensing offers a unique potential to provide synoptic water quality monitoring of large water bodies on a daily basis. This approach has proven to be extremely valuable to better understanding cause and effect relationships between observed phenomena and their forcing functions. Several investigators have developed or applied algorithms to retrieve water quality parameters in Lake Erie including chlorophyll-a (Binding et al., 2012; Shuchman et al., 2013; Lesht et al., 2013), water clarity (Binding et al., 2007, 2015), inorganic mineral concentrations (Binding et al., 2012; Shuchman et al., 2013), dissolved organic carbon (Shuchman et al., 2013), and cyanobacteria presence (Vincent et al., 2004; Becker et al., 2009; Wynne et al., 2008; Sayers et al., 2016; Ho et al., 2017). These remote sensing products have provided valuable new insights and an ability to quantify broad changes in water quality in Lake Erie. While useful, these algorithms are limited in their ability to derive more sophisticated water quality information such as phytoplankton functional types (PFT) or algal group classifications. More advanced multi-spectral and hyperspectral algorithm methodologies with precise model parameterizations will be needed in order to accurately recover these more detailed water quality products.

Bio-optical algorithms, both empirical and semi-analytical, relate water quality properties to the spectral light field. In complex inland and coastal waters, bulk optical properties are controlled by the abundance and composition of the optically active constituents (OACs) which are comprised of phytoplankton, colored dissolved organic matter (CDOM), and non-algal particles (Werdell et al., 2018). The abundance of OACs are related to observed water leaving radiance, an apparent optical property (AOP), through their unique inherent optical properties (IOPs) which at the most fundamental level include spectral absorption and scattering (Morel and Prieur, 1977). The IOP spectral shapes, which dictate the spectral shape of observed water leaving radiance, can be highly variable depending on the specific types of OACs that are in the water column (Moore et al., 2014). For example, different phytoplankton types can have distinctly different light absorbing pigment compositions that have distinct spectral shapes (Bricaud et al., 2004; Ciotti et al., 2002). As phytoplankton group composition changes over the course of a year or between years, so do the underlying IOPs. Remote sensing algorithms with the objective of identifying PFTs and other parameters must take into account the variability in spectral IOPs of the observed water body (IOCCG, 2014; Mouw et al., 2017).

Documented observations of IOPs in Lake Erie are relatively sparse in respect to their spatial and temporal variability. Binding et al. (2008) reported some of the first IOP measurements for Lake Erie by analyzing laboratory derived absorption coefficients for several months in 2004 and 2005. O'Donnell et al. (2010) made in situ IOP and AOP measurements for a two-day period in September 2007. Recently, Moore et al. (2017) reported a full suite of IOP and AOP observations for the western basin of Lake Erie acquired in mid-August for both 2013 and 2014 with the goal of characterizing the optical properties during the cyanobacteria bloom peak. While these measurements have been valuable for the development of remote sensing water quality retrieval algorithms, they are limited in their temporal scales. It is unclear from the presently reported IOP and AOP values how representative they are over the ice-free period and how consistent they are between years. Understanding the natural variability in IOPs over an entire season is important for remote sensing algorithms that require known values for algorithm parameterization. Semi-analytical algorithm frameworks reported by Binding et al. (2012), Shuchman et al. (2013), and Simis et al. (2005) all make assumptions about mass specific absorption and scattering coefficients computed as mean values from limited datasets. How these algorithms, using "default" parameterizations, perform over the vegetative season is unclear. Better understanding of the seasonal IOP and AOP variability will allow for the refinement of these approaches to provide more robust retrievals over long time periods.

In this study, we investigate the spatial and temporal variability of several IOP variables at weekly, monthly, and annual scales over the vegetative season. The aim of this study is to 1) present a new IOP and AOP dataset for Lake Erie at unprecedented temporal intervals (weekly); and 2) identify significant patterns and trends in IOPs and AOPs throughout the vegetative season.

Methods

Study area

Sampling was conducted on a near weekly basis in Lake Erie from May through October of 2015 and 2016, collecting data from 6 master stations (WE2, WE4, WE6, WE8, WE12, and WE13) shown on Fig. 1. Station WE15 was sampled on a near weekly basis beginning in July 2015. Data was collected from two other stations but for less extensive time periods, and were not used in this analysis (WE9 was only sampled in 2016 and WE14 was only sampled from July through October of 2015). At each station instruments were deployed to measure IOPs/AOPs and water samples were collected for basic water quality measures, i.e., chlorophyll-a (Chl-a), phycocyanin (PC), colored dissolved organic material (CDOM), and total and fixed suspended solids (TSS and FSS, respectively).

Biogeochemical laboratory data

Water samples from the top meter of the water column were collected with a Niskin bottle and poured into three sample bottles simultaneously, repeating until sample bottles were full. Samples for pigment analyses were filtered onto Whatman GF/F filters, extracted with appropriate solvent, and analyzed fluorometrically. For Chl-a samples, filters were extracted with N,N-dimethylformamide (Speziale et al., 1984) and analyzed on a Turner Designs fluorometer calibrated with Chl-a a standards. Filters for PC determination were extracted in phosphate buffer (Ricca Chemical, pH 6.8) using two freeze–thaw cycles, followed by sonication (Horváth et al., 2013). Relative fluorescence was measured on a Turner Aquafluor fluorometer and converted to PC concentration using a series of dilutions of a commercial standard (Sigma-Aldrich). The concentration of total suspended solids (TSS) was determined gravimetrically after filtering the sample through a pre-dried, pre-weighed Whatman GFC 47-mm filter. The filter was then combusted for 4 h at 450 °C, cooled, and reweighed to measure volatile suspended solids (VSS; APHA, 1998). The concentration of fixed suspended solids (FSS), the non-organic sediments in the water sample, was determined as the difference between TSS and VSS concentrations. Lake water was filtered under low vacuum on pre-rinsed (1 N HCl) 0.2 µm pore size Millipore membranes for CDOM absorption measurements and refrigerated (4 °C) in the dark until analyzed. Absorbance of the filtered water was measured in a 10 cm quartz cuvette from 400 to 700 nm at 2 nm increments with a dual beam spectrophotometer (Perkin Elmer, lambda 40), with deionized water used as the reference (Effler et al., 2010). CDOM spectral slope (S) was calculated using a nonlinear exponential fit over the wavelength range from 400 to 500 nm (Twardowski et al., 2004) using MATLAB code provided by the Maine In-Situ Sound & Color Lab (http://misclab.umeoce.maine.edu).

Optical data

IOP data were collected using a WET Labs spectral absorption and attenuation meter (ac-s) (WET Labs, Inc.). This meter was deployed over the side of the research vessel, along with a CTD instrument (Sea-Bird Scientific) to record temperature and depth, and lowered to just above the lake floor, collecting data throughout the water column. The ac-s measured spectral attenuation and absorption at 86 wavelengths from approximately 400 nm to 740 nm. In-lab calibration using purified Milli-Q water was conducted according to WET Labs instructions on a
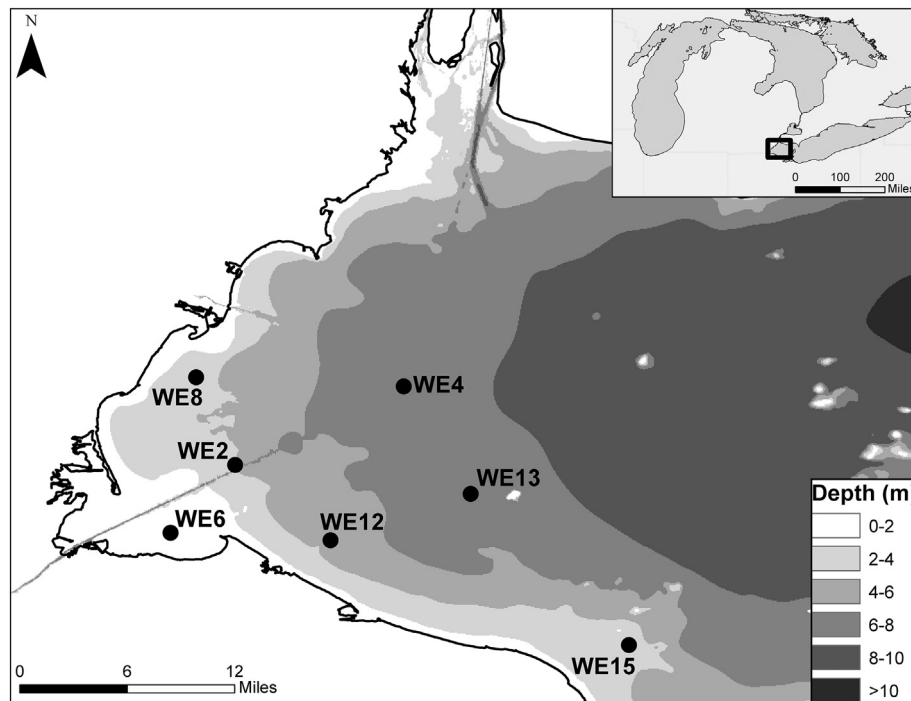
Fig. 1. Station names and locations from 2015 and 2016 weekly data collections. Stations sampled regularly (weekly) are shown as black dots. Basin bathymetry is shown as varying shades of gray with darker colors indicating deeper water depth.

regular basis between field cruises in order to track instrument drift (https://www.seabird.com/transmissometers/ac-s-spectral-absorption-and-attenuation-sensor/).

A Satlantic HyperPro II profiler (Satlantic, Inc.) was deployed at the stations to collect upwelling radiance (L_u) and downwelling irradiance (E_d) throughout the water column. The profiler was deployed off the side of the research vessel and collected data while slowly free-falling through the water column. ProSoft software (v7.7, Satlantic, Inc.) was used to process the HyperPro data for analysis, binning data to 0.3 m depth intervals. Processing the raw data files to level 4 generated diffuse attenuation coefficients through the water column (Sea-Bird Scientific, 2017). Apparent optical depth, the depth where 90% of water leaving radiance originates (Gordon and McCluney, 1975), was calculated as 1.3 divided by the wavelength-specific attenuation coefficients derived from the profiler's E_d sensor (Werdell and Bailey, 2005; Bailey and Werdell, 2006).

Hyperspectral above-water radiance was collected using a Satlantic HyperGun (Satlantic, Inc.). This instrument collects radiance at 137 channels covering a spectral range of approximately 350–800 nm with an approximate spectral resolution of 3 nm and a 3-degree field of view. Upwelling radiance (L_u, W/m²/sr^{-1}/nm^{-1}) was measured at approximately 150° relative to the solar azimuth at the time of measurement (Mobley, 1999). The HyperGun was pointed at the water's surface at 40° from nadir and measurements were taken for 15 s. The HyperGun was shifted 90° upward (~40° from zenith) and radiance measurements were taken of the sky, L_{sky}, for approximately 15 s. The measured radiance of an 18% reflective panel was collected at approximately 40° from nadir for approximately 15 s. Additionally, care was taken to avoid shadows, sun glint, and floating debris when collecting data. HyperGun data were downloaded from the instrument, radiometrically calibrated and dark-offset corrected using the most recent factory calibration file. Irradiance (E_d, W/m²/nm^{-1}) was calculated as the radiance of the panel divided by the known reflectance of the panel (0.18) and multiplied by π (Mobley, 1999; Mueller, 2003). The water leaving radiance (L_w) was corrected for diffuse sky contamination using the following equation: $L_w = L_u - 0.028 * L_{sky}$ (Mobley, 1999), where 0.028 is taken to be the reflectivity of the water's surface. The remote sensing

reflectance ($R_{rs}(\lambda)$, sr^{-1}) was calculated as L_w divided by E_d. A Savitzky-Golay filter (Savitzky and Golay, 1964) was used to smooth the noise in the spectra.

Raw data from the ac-s instrument was processed through the WET Labs Archive Processing (WAP) tool (v4.37, WET Labs, Inc.). Outlier calibration spectra caused by bubbles in the water supply were removed, the average calibration absorption and attenuation spectra were calculated, and temperature corrected. Field data from the ac-s and CTD instruments were merged, correcting for time lags. The ac-s absorption and attenuation data were interpolated to common wavelengths (WET Labs Inc., 2011). Absorption tube scattering corrections were applied to the ac-s data to account for overestimations of the absorption coefficients due to uncollected scattered light (Röttgers et al., 2013). Temperature corrections were applied based on the temperature retrieved from the CTD instrument (Sullivan et al., 2006) and instrument drift corrections were applied based on the most recent instrument pure water calibration spectra. Additional checks were performed on ac-s data, resulting in the removal of data meeting any of the following criteria: absorption is greater than attenuation, absorption or attenuation less than −0.005 (due to instrument precision, negative data values greater than −0.005 were set to zero), or saturated backscattering data (https://www.seabird.com/transmissometers/ac-s-spectral-absorption-and-attenuation-sensor/). All remaining data were binned by depth at intervals of 0.1 m.

After initial processing of the field data, additional steps were taken to prepare the data for final analysis. Hyperspectral IOP data were aggregated over the apparent optical depth from each station to best represent the water that was visible to satellite imaging sensors. If no HyperPro profiler data were available on a given date, the season-long average apparent optical depth for that station was used. The season-long average was used in place of the most recent sampling because a visual inspection of the optical depth spectra through the season revealed substantial variability from week to week. A minimum depth of 1 m was used to ensure that enough field data was included in the aggregated output. Station WE6 was too shallow to calculate attenuation, resulting in no apparent optical depth data. For this station, all IOP data were aggregated over the top 1 m. After apparent optical depth

aggregation, data were removed that failed a few basic checks: if the absorption or attenuation values were greater in red (640 nm) than in blue (420 nm) or if the ratio of absorption or attenuation at 500 nm to 440 nm was <1. A Savitzky-Golay filter was used to smooth noise in the spectral curves (Savitzky and Golay, 1964). In the approximately 7% of cases where the beam attenuation spectral curves did not follow the expected exponential decay trend from 400 to 420 nm, the curve fit function in Python's SciPy module was used to correct the shape of the curve (Jones et al., 2001). All optical data are available by request from the NOAA Great Lakes Environmental Research Laboratory (GLERL).

Data analysis

Scattering (b) was derived from the ac-s meter-generated absorption (a) and beam attenuation (c) data according to Eq. (1):

$$c(\lambda) = a(\lambda) + b(\lambda) \tag{1}$$

Absorption can be partitioned into constituent components according to Eq. (2):

$$a_t(\lambda) = a_w(\lambda) + a_{pg}(\lambda) \tag{2}$$

where a_w is the absorption due to pure water and a_{pg} is the absorption due to particulates, a_p, plus the absorption due to CDOM, a_g. The output from the ac-s has already had pure water absorption removed (WET Labs Inc., 2011), leaving only the combined particulate and CDOM absorption as the constituent parts in the spectra. Using the lab-derived CDOM absorption at 400 nm ($a_{CDOM}400$) and the calculated CDOM spectral slope (S_{CDOM}), the CDOM absorption spectra were derived according to Eq. (3) (Twardowski et al., 2004):

$$a_{CDOM}\lambda = a_{CDOM}400 * e^{-S(\lambda - 400)} \tag{3}$$

Subtracting the CDOM absorption spectra from the a_{pg} spectra results in the particulate absorption spectra ($a_p(\lambda)$), which is the absorption due to algal and non-algal particles in the water. Particulate beam attenuation ($c_p(\lambda)$) can then be derived according to Eq. (4):

$$c_p(\lambda) = a_p(\lambda) + b_p(\lambda) \tag{4}$$

where b_p is the scattering coefficient derived from Eq. (1). Because CDOM scattering is assumed negligible or non-existent and pure water scattering has already been removed, the calculated total scattering is inherently due to in water particulates.

Several IOP optical proxies were generated from the derived a_p spectra. The particulate absorption PC line height (PCLH$_{ap}$) was used as a proxy for the presence of PC and was derived using a variation of the absorption line height methods described in Roesler and Barnard (2013). PCLH$_{ap}$ was calculated as the difference between a_p at 620 nm (the PC absorption peak; Simis et al., 2005; Roy et al., 2011) and the baseline absorption at 620 nm. The mass specific phytoplankton absorption coefficient at 665 nm ($a^*_{ph}665$) was used as a proxy for phytoplankton size/type and was derived as the particulate absorption chlorophyll line height (CHLLH – described below) divided by the corresponding lab-derived Chl-a concentration for each sample. The absorption at 665 nm was used instead of 676 nm as used by Slade and Boss (2015) because several relevant remote sensing algorithms including those proposed by Simis et al. (2005) and Binding et al. (2012) use specific phytoplankton absorption around this band in their respective bio-optical models, which were developed in cyanoHAB conditions.

The absorption line height approach used in the calculation of PCLH$_{ap}$ and $a^*_{ph}665$ is fully described in Roesler and Barnard (2013) as well as in Slade and Boss (2015). Briefly, the absorption line height method calculates the difference of observed particulate absorption at a reference wavelength above a baseline absorption value. This approach allows for the estimation of pigment absorption in the presence of other absorbing constituents, which in the case of a_p are other non-algal particles. The baseline absorption value approximates the absorption from non-algal particles and is derived using a linear equation of the form:

$$a_{BL}(\lambda_{ref}) = \frac{a(\lambda^+) - a(\lambda^-)}{\lambda^+ - \lambda^-} * (\lambda_{ref} - \lambda^-) + a(\lambda^-) \tag{5}$$

where λ_{ref} is the reference wavelength (620 nm for PCLH$_{ap}$ and 665 nm for CHLLH), λ^- is the wavelength at baseline start (600 nm for PCLH$_{ap}$ and 650 nm for CHLLH), and λ^+ is the wavelength at baseline end (648 nm for PCLH$_{ap}$ and 715 nm for CHLLH).

The line height absorption is then calculated as:

$$a_{LH}(\lambda_{ref}) = a(\lambda_{ref}) - a_{BL}(\lambda_{ref}) \tag{6}$$

The particulate beam attenuation spectral slope (γ) was calculated using a non-linear power law fit over the wavelength range from 400 to 500 nm (Boss et al., 2001; Slade and Boss, 2015) using MATLAB code provided by the Maine In-Situ Sound & Color Lab (http://misclab. umeoce.maine.edu). The particulate beam attenuation spectral slope represents the variability in particle size distributions (Boss et al., 2001).

Results

Large variations in water constituents (Chl-a, PC, FSS) were observed over the course of the two-year study period. Table 1 summarizes the range, mean, and median Chl-a, PC, and FSS values for 2015, 2016, and combined for both years. The table represents data from all sites with the exception of one sample from station WE8 on August 10, 2015 due to extremely large concentrations of surface scum (e.g. 6784 mg/m^3 Chl-a and 8228 mg/m^3 PC). Additionally the optical proxy values are also summarized on the table and are described in detail in subsequent sections.

Values of Chl-a, PC, and FSS were different between 2015 and 2016 (Fig. 2). Median Chl-a values in August 2015 were more than double those in August 2016. Higher median Chl-a was also observed in 2015 for July and September while similar values were observed between years in May and October (Fig. 2 top panel). Much larger PC values were observed in July, August, and September 2015 compared to values in 2016 (Fig. 2 middle panel). Lastly, FSS was highly variable for both years with the largest values in 2015 occurring in June and October while for 2016 the largest values occurred from August–October (Fig. 2 bottom panel).

Mean monthly IOP parameter (absorption, scattering, and beam attenuation) magnitudes displayed a wide range in variability for WBLE in 2015 and 2016 (Fig. 3 left panels). For example, IOP magnitudes were quite similar for August in both 2015 and 2016 while magnitude differences between October 2015 (low magnitude) and 2016 (high magnitude) were very large. In fact, the magnitudes in October 2015 and 2016 represent the minimum and maximum mean monthly IOP values for both years combined. Even with the large differences observed in October, magnitudes in all three IOPs were generally higher in 2015 (solid lines) than 2016 (dashed lines).

Spectral differences were observed for all three IOP parameters (Fig. 3 right panels) by month and year with the largest differences occurring between October 2015 and 2016 again spanning the range of all other months and years. The largest differences occur in the blue wavelengths (~400–450 nm) where the decreasing slopes vary by month and year. Conversely, the normalized absorption curves (Fig. 3 right middle panel) for September 2015 and 2016 are nearly identical, both of which exhibit a peak at the Chl-a absorption feature at approximately 665 nm. This feature also appears in both August 2015 and 2016 coinciding with cyanoHAB bloom events. However, very little visual evidence of the Chl-a absorption feature at 665 nm exists in October 2015 and 2016 or in

Table 1
Summary statistics for the four inherent optical properties (a_{ph}*665, $PCLH_{ap}$, S_{CDOM}, γ) and laboratory biochemical parameters (Chl-a, PC, and FSS). Summary statistics include range, mean, and median values for each year and combined for both years.

Parameter	Units	2015			2016			Combined		
		Range	Mean	Median	Range	Mean	Median	Range	Mean	Median
a_{ph}*665	m^2/mg^{-1}	<0.001–0.015	0.003	0.003	<0.001–0.009	0.004	0.004	<0.001–0.015	0.004	0.003
$PCLH_{ap}$	m^{-1}	<0.001–0.130	0.017	0.010	<0.001–0.11	0.008	0.003	<0.001–0.13	0.012	0.006
S_{CDOM}	nm^{-1}	0.014–0.020	0.017	0.017	0.011–0.026	0.017	0.018	0.011–0.026	0.017	0.017
γ	nm^{-2}	0.21–2.05	0.91	0.84	0.49–2.26	1.01	1.01	0.21–2.26	0.96	0.93
Chl-a	mg/m^3	1.01–352.60	43.95	28.32	1.27–114.6	15.63	7.95	1.01–352.6	29.84	12.55
PC	mg/m^3	0.00–514.20	26.07	9.45	0.01–42.24	2.62	0.66	0.0–514.2	14.25	1.43
FSS	g/m^3	1.07–129.60	12.97	7.24	0.28–51.88	8.40	6.28	0.28–129.6	10.75	6.43

July 2015 indicating strong absorption by CDOM or non-algal particles relative to phytoplankton absorption in this wavelength region. The normalized spectral scattering coefficients (Fig. 3 right bottom panel) display two distinct groups of spectral shapes with September 2016 and October 2016 very similar to each other and yet quite different from the other months and years.

Spatial variability in mean IOP magnitude (Fig. 4 left panels) was observed between five stations in the WBLE 2015–2016 dataset. The maximum values for all three parameters were observed at WE12 followed closely by WE2. Of the regularly sampled stations, these two stations were in closest proximity to the mouth of the Maumee River. A distinct separation in beam attenuation and scattering between stations WE12 and WE2 and all other stations was evident. Station WE4 exhibited the lowest absorption for all spectral regions and lowest beam attenuation in the ~400–500 nm range. In contrast, WE8 displays the lowest scattering but relatively large absorption values.

Spatial differences in shape are clearly observed in the normalized IOP spectra (Fig. 4 right panels) between the five stations in the 2015–2016 dataset. Stations WE4 and WE13 exhibited nearly identical beam attenuation spectra (Fig. 4 right top panel) where as WE2, WE12, and WE8 were different. The normalized absorption spectra (Fig. 4 right middle panel) for stations WE2 and WE8 were identical

while the remaining stations exhibit slight shape differences in the short blue (400–450 nm) spectral region. The Chl-a absorption feature at 665 nm was observed at all stations with slight differences in shape. The PC absorption peak at 620 nm was also observable at all stations. Two distinct groupings were evident in the normalized spectral scattering (Fig. 4 right bottom panel) spectra with stations WE2, WE12, and WE8 showing very similar shape while WE4 and WE13 were similar. The two groups exhibited clearly different spectral scattering slopes.

The mass specific phytoplankton absorption coefficient at 665 nm, a_{ph}*665, was analyzed as a proxy for phytoplankton/algal community (i.e. size) variability which displayed seasonal and annual differences in median values (Fig. 5 top panel). The mean, median, and range of a_{ph}*665 values are displayed in Table 1. Using the Mann Whitney *U* test (Mann and Whitney, 1947), significant differences from the overall median a_{ph}*665 values were observed in 2015 for May ($p < 0.001$), August ($p < 0.001$), September (p-0.024), and October ($p < 0.001$). Significant differences from the overall median were also identified in 2016 for May ($p = 0.001$), June ($p = 0.008$), September ($p = 0.006$), and October ($p = 0.021$). The largest a_{ph}*665 values for both 2015 and 2016 were observed in May and exhibited steady declines through August as the phytoplankton community shifts from predominantly diatoms to colonial cyanobacteria (Bosse et al., 2019; *this issue*). While May
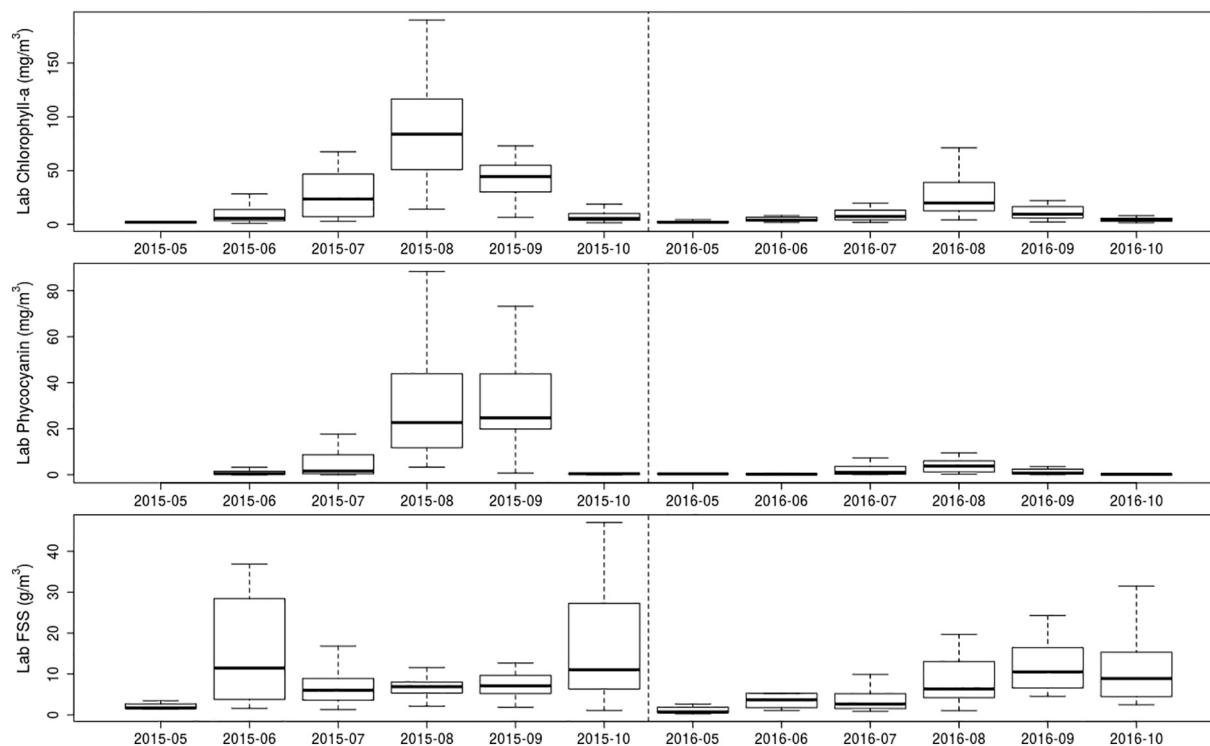

Fig. 2. Temporal patterns of chlorophyll-a (top panel), phycocyanin (middle panel), and fixed suspended solids (bottom panel) in western Lake Erie expressed as boxplots where the black horizontal line is the median, the bottom and top of the box are the first and third quartiles respectively, and the horizontal gray lines below and above the box are the minimum and maximum values respectively. Monthly median values for 2015 (left half) and 2016 (right half) are shown in all three panels.
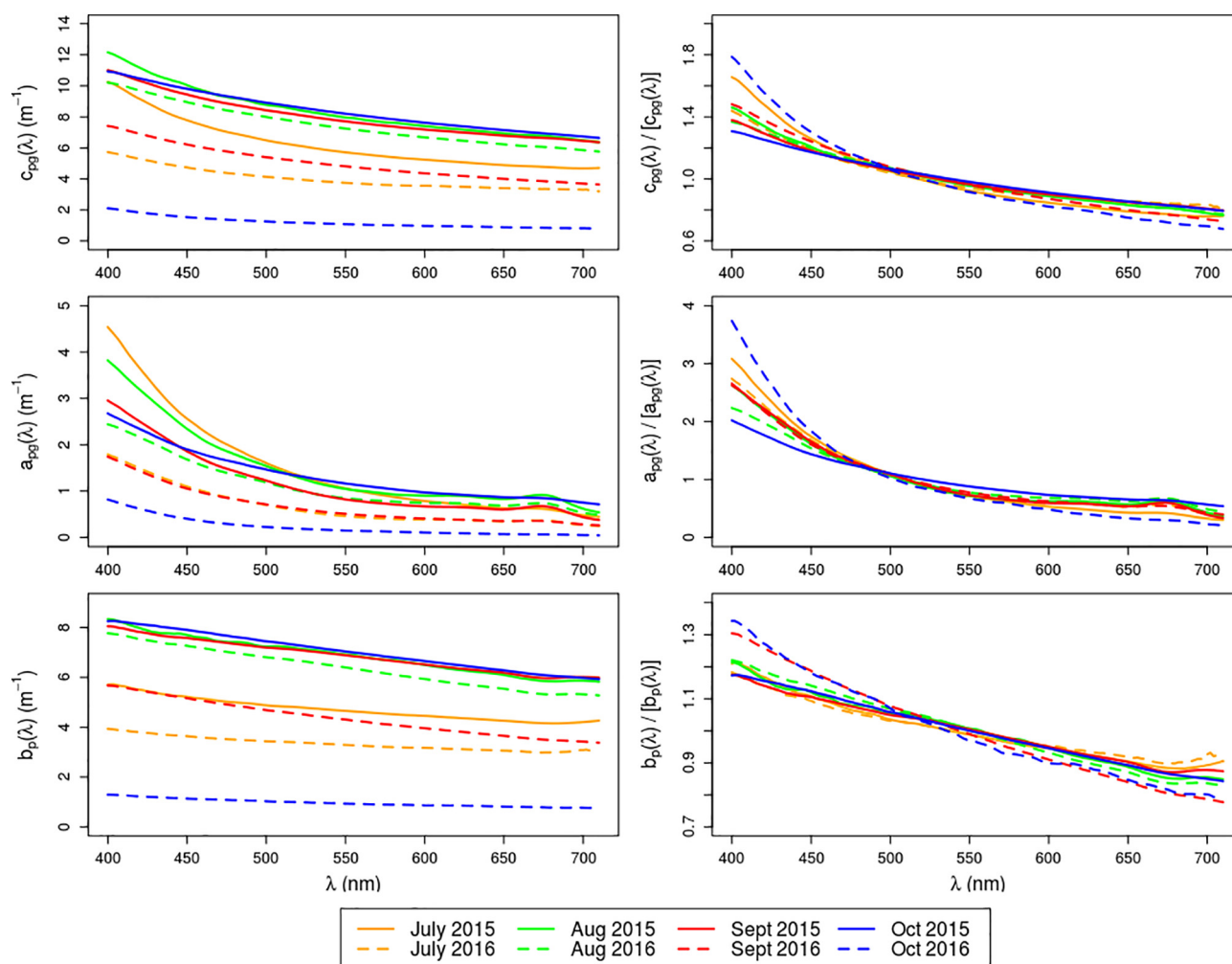
Fig. 3. Monthly mean beam attenuation, absorption, and scattering coefficients for 2015 and 2016. Absolute values are shown in the left panels while mean normalized spectra are shown in the right panels. Lines are colored by month where solid lines represent 2015 data and dashed lines 2016 data. Note absolute value spectra (left panels) are on different y-axis scales.

$a_{ph}*665$ were largest for both years, they were significantly different from each other (p = 0.016) with greater median values occurring in 2015. For 2015, $a_{ph}*665$ values increased from August through October while in 2016 the values continue to decrease from August through October. The difference in seasonal trends between years is a result of significantly different values of $a_{ph}*665$ in August (2015 lower than 2016, p < 0.001) and October (2015 > 2016, p = 0.004) respectively. Large variability in monthly $a_{ph}*665$ values are observed in both 2015 and 2016, however, the variability is not consistent between years. For example, large variability $a_{ph}*665$ was observed in June 2015 while there was little variability in June 2016.

There were no significant differences in combined study (all 2015 and 2016 data) median $a_{ph}*665$ values between sampling stations (Fig. 5 middle panel). Stations also exhibited very similar variability in $a_{ph}*665$ with the exception of WE4 which displayed a larger degree of variance relative to other stations. Additionally, all stations exhibited median values similar to the combined study period median value (0.003 m^2/mg^{-1}). Two stations, WE12 and WE15, displayed significant differences (WE12 p = 0.05, WE15 p = 0.02) in $a_{ph}*665$ between 2015 and 2016 while all others were not significantly different between years (Fig. 5 bottom panel). However, with the exception of WE6, all stations exhibited greater median values in 2016 compared with 2015. Annual variability in $a_{ph}*665$ for each station was inconsistent as some stations showed similar variability between 2015 and 2016 (e.g. WE15) while others (e.g. WE6) were very different between years. Finally, there

were no significant differences between sampling station annual median $a_{ph}*665$ values and the overall combined median value.

The particulate absorption PC line height (PCLH$_{ap}$) was used to examine temporal and spatial variability of PC absorption as a proxy for cyanobacteria abundance (Fig. 6). Comparisons between PCLH$_{ap}$ values and coincident PC extracted concentrations revealed a strong positive relationship (Pearson's correlation = 0.72) (Fig. 6). While PCLH$_{ap}$ and PC concentration were positively correlated, a high degree of variability was also observed, indicating PCLH$_{ap}$ may be sensitive to other absorbing pigments. For example, Chl-a exhibits a slight absorption feature in the same spectral region (~620 nm) as PC absorption (Roy et al., 2011) which contributes to the PCLH$_{ap}$ in addition to PC. It also should be noted that the spread observed in Fig. 6 could also be an effect of pigment packaging where the PCLH$_{ap}$ was derived from particulate absorption where pigments remain bound in the cells/colonies while the laboratory PC has been extracted as is measured in solution.

The mean, median, and range of PCLH$_{ap}$ values are also displayed in Table 1. Significant differences (see Fig. 7) from the overall study median PCLH$_{ap}$ value (0.006 m^{-1}) were observed in 2015 for May (p = 0.005), August (p < 0.001), September (p < 0.001), and October (p = 0.02), while differences were also identified in 2016 for June (p = 0.004), September (p = 0.009), and October (p = 0.011). The monthly trends in PCLH$_{ap}$ values were generally consistent between 2015 and 2016 with both years showing low values in May increasing through August followed by a steady decline through October. Additionally, the
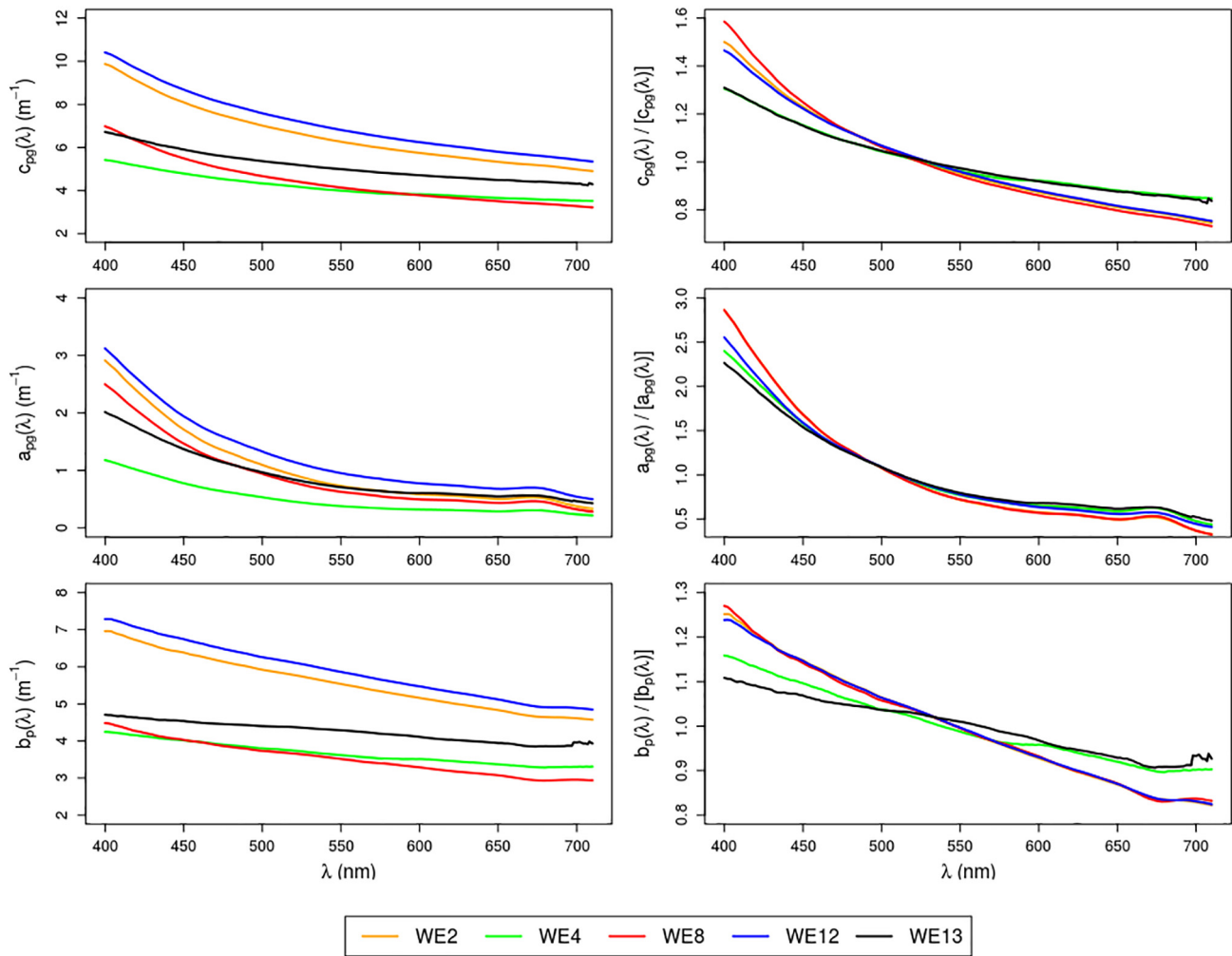
Fig. 4. Station mean (2015 and 2016 combined) beam attenuation, absorption, and scattering coefficients. Absolute values are shown in the left panels while mean normalized spectra are shown in the right panels. Lines are colored by station location. Note absolute value spectra (left panels) are on different y-axis scales.

highest maximum values for 2015 and 2016 were observed in August coinciding with the peak cyanoHAB period (Wynne and Stumpf, 2015, Sayers et al., this issue). While the seasonal trends were similar, the degree of $PCLH_{ap}$ increase from May to August was larger in 2015 than in 2016 indicating much greater abundance of cyanobacteria presence in 2015 than 2016. This is confirmed through a comparison of monthly median $PCLH_{ap}$ values between 2015 and 2016, where both August and September 2015 values were significantly greater than the 2016 August and September $PCLH_{ap}$ values (August $p = 0.013$; September $p < 0.001$).

Spatial variability in the combined two-year study period sample station median $PCLH_{ap}$ values was observed (Fig. 7 middle panel), with station WE4 exhibiting significantly lower median $PCLH_{ap}$ values than WE6 ($p < 0.001$). Stations WE12, WE13, WE15, WE2, WE6, and WE8 did not have significantly different $PCLH_{ap}$ values over the two-year period. Moreover, all stations with the exception of WE4 showed comparable $PCLH_{ap}$ variability over the two-year study period. Additionally, the median $PCLH_{ap}$ value for WE4 was significantly smaller ($p = 0.008$) than the overall study median value while WE6 was significantly greater ($p < 0.001$). There were also significant differences in median annual $PCLH_{ap}$ values for stations between 2015 and 2016 (Fig. 7 bottom panel). For example, stations WE12 ($p = 0.008$), WE15 ($p = 0.012$), and WE2 ($p = 0.003$) all had significantly lower $PCLH_{ap}$ values in 2016 than in 2015, while WE13, WE4, WE6, and WE8 had no difference between years.

The CDOM absorption spectral slope, S_{CDOM}, was analyzed to characterize the spatial and temporal variability of CDOM composition in western Lake Erie. The mean, median, and range of S_{CDOM} values are also displayed in Table 1. While S_{CDOM} values exhibited similar range and median values overall for 2015 and 2016, significant temporal differences in S_{CDOM} were observed between 2015 and 2016 (Fig. 8 top panel). June and July median S_{CDOM} values were significantly lower in 2015 than in 2016 while values were similar in May, August, September, and October (June $p = 0.015$, July $p = 0.001$). Intra-monthly variability in S_{CDOM} values was consistent between 2015 and 2016 except for August and September where variability was larger in 2016 than in 2015.

While significant temporal differences in S_{CDOM} were documented, there were no significant differences in combined 2015–2016 median values for each station (Fig. 8 middle panel). Variance in station median S_{CDOM} values was also similar with WE4 showing a slightly higher degree of variability than the other stations. Because of the increased variance in S_{CDOM} at WE4, its median value was significantly smaller than the overall combined study median value (0.017 nm^{-1}, $p = 0.036$). There was also no significant difference between median S_{CDOM} values between years for each station, although the minimum and maximum values were quite different for some stations between 2015 and 2016 (e.g. WE15) while others were not (e.g. WE2) (Fig. 8 bottom panel).

In order to understand the spatial and temporal variability in scattering by particles (suspended solids and phytoplankton), the particulate beam attenuation (c_p) spectral slope (γ) was analyzed (Fig. 9 top
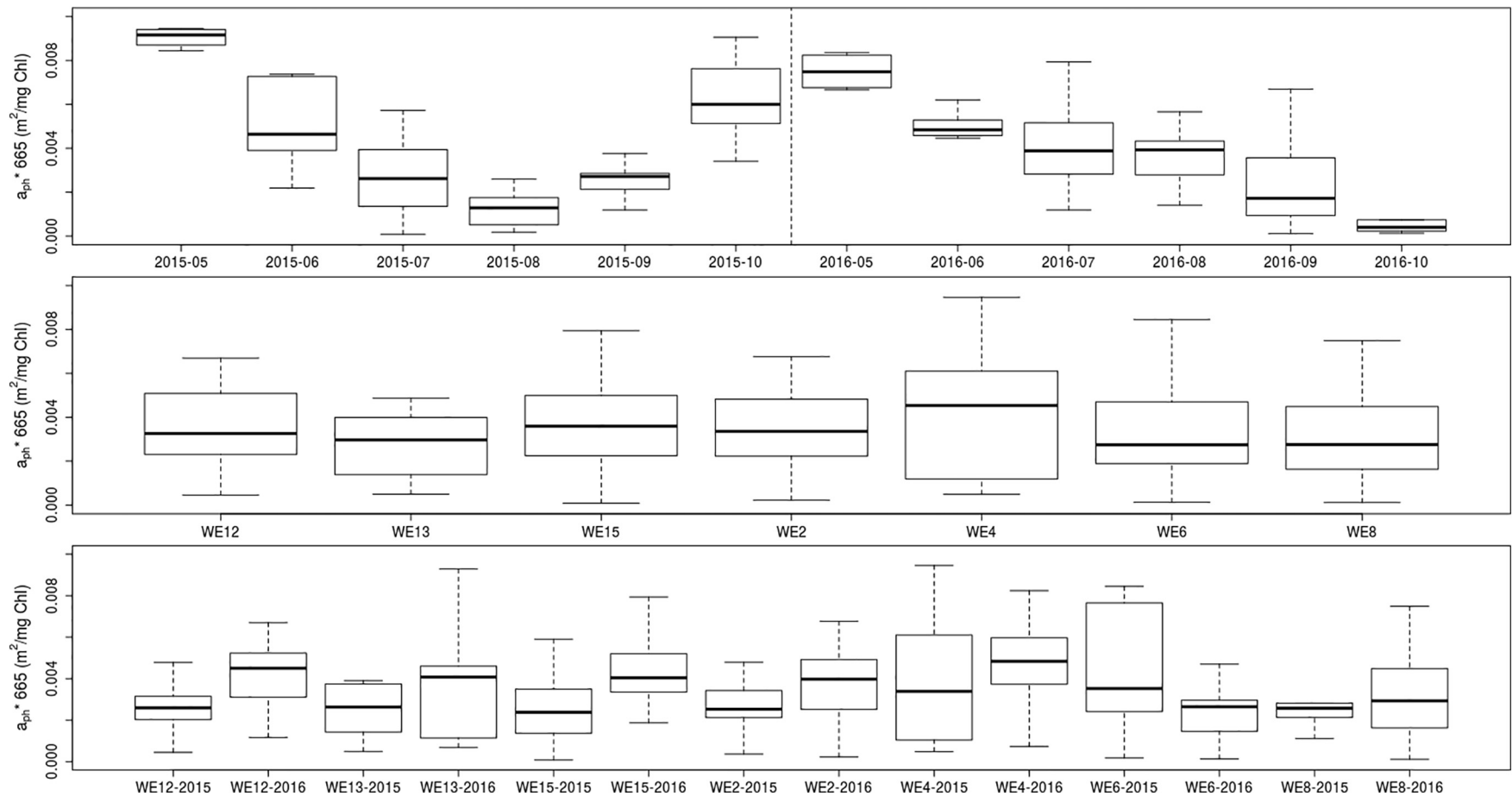
Fig. 5. Spatial and temporal patterns of a_{ph}*665 in western Lake Erie expressed as boxplots where the black horizontal line is the median, the bottom and top of the box are the first and third quartiles respectively, and the horizontal gray lines below and above the box are the minimum and maximum values respectively. Monthly median values for 2015 (left half) and 2016 (right half) are shown in the top panel. Station median values for the combined 2015–2016 dataset are shown in the middle panel. Annual station median values are shown in the bottom panel.
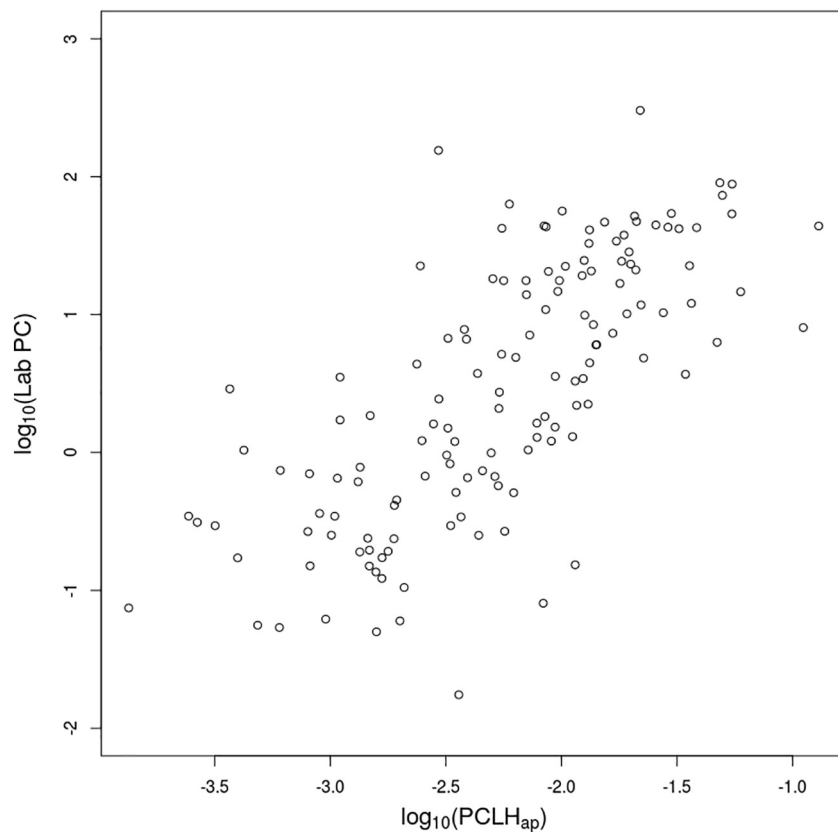
Fig. 6. Comparison between particulate absorption phycocyanin line height (PCLH$_{ap}$) (x-axis) and laboratory extracted phycocyanin concentration (Lab PC) (y-axis). Note the log$_{10}$ scales.

panel). The mean, median, and range of γ values are also displayed in Table 1. Differences between months in 2015 and 2016 were evident, most notable where July 2015 was significantly greater than July 2016 (p = 0.01), while 2016 September (p < 0.001) and 2016 October (p = 0.002) were larger than both months in 2015. Very similar values were observed in both August 2015 and 2016 corresponding to the dominant cyanoHAB occurrence period. Intra-monthly variance in γ is greatest in May and October for both years corresponding to elevated river discharge and resuspension events. The single largest monthly variance occurred in July 2015 during the cyanoHAB initiation period where there were several large precipitation events resulting in very high discharge rates from the Maumee River (Michalak et al., 2013).

Spatial differences in γ were observed between stations for the combined 2015–2016 dataset (Fig. 9 middle panel) most notably at WE4 which had median γ values significantly lower than the other stations (p < 0.001). Stations WE13 and WE4 exhibited the lowest γ values and are located the furthest distance offshore relative to the Maumee River discharge plume. The highest values of γ were observed at WE8, which also exhibited the greatest variability. Comparison of median γ values for each station between years suggested general similarity with the exception of WE4 which had significantly lower values in 2015 than in 2016 (p = 0.007). While stations generally exhibited similar median values between years, there were differences in the range of γ values observed at each station. For example, maximum γ values at WE6 were approximately 60% greater in 2015 than in 2016 while maximum values were almost 50% greater in 2016 than 2015 for WE13 (Fig. 9 bottom panel).

In light of the large observed variability in western Lake Erie IOPs and optical proxies, it is expected that similar differences in measured remote sensing reflectance (R$_{rs}$) would be observed. Mean R$_{rs}$ spectra were calculated for each month (using data from all stations) in 2015 and 2016 respectively and are shown in Fig. 10 (red lines). Variability in monthly spectra are also shown in the gray-black regions around

the mean spectra where each color represents a percentage of measured R$_{rs}$ values, following the method described by Hochberg et al. (2003) (light gray = 2.5–97.5%, medium gray = 12.5–87.5%, dark gray = 25–75% and black = 37.5–62.5%). Note, no R$_{rs}$ data were recorded in May and October for 2016 due to the instrument undergoing maintenance. Within-year variability in mean spectral shape is evident in both 2015 and 2016. Early season (i.e. May–June) mean spectra for both years exhibit shapes typically associated with diatom presence (i.e. a wide and rounded peak between 500 and 600 nm), while mean spectra with cyanobacteria spectral features (e.g. troughs around 620 nm (PC absorption) and 676 nm (Chl-a absorption); peak around 705 nm (particle scattering)) occur in August for both years. A wide range in spectra magnitude is observed in June and October 2015, which is due to the presence of large sediment plumes characteristic of the elevated reflectance values in the red spectral region (i.e. 600–700 nm).

In addition to the monthly variability in R$_{rs}$, spatial variability was also evident. Fig. 11 is an example of the variability in R$_{rs}$ between stations WE4 (top panels) and WE6 (bottom panels). Absolute R$_{rs}$ values are shown in the left panels while normalized R$_{rs}$ spectra are shown in the right panels. Reflectance spectra were normalized (nR$_{rs}$(λ)) by dividing each spectra by its root sum of squares (Wei et al., 2016). A difference in the range in R$_{rs}$ magnitude between WE4 and WE6 is apparent, with WE6 exhibiting much higher R$_{rs}$ in the 550–700 nm spectral region likely the result of substantial sediment plumes. The normalized spectra (right panels) show a clear difference in spectral shapes between the stations with WE6 exhibiting a mean spectra with features characteristic of cyanobacteria while WE4 is more typical of other phytoplankton assemblages. Both stations display spectra associated with surface scums events (peak ~705 nm) however; these scums appear to be more frequent at WE6.

Because of the similar variability observed in both IOPs and AOPs (R$_{rs}$) and the fact that R$_{rs}$ shape and magnitude are a function of IOPs,
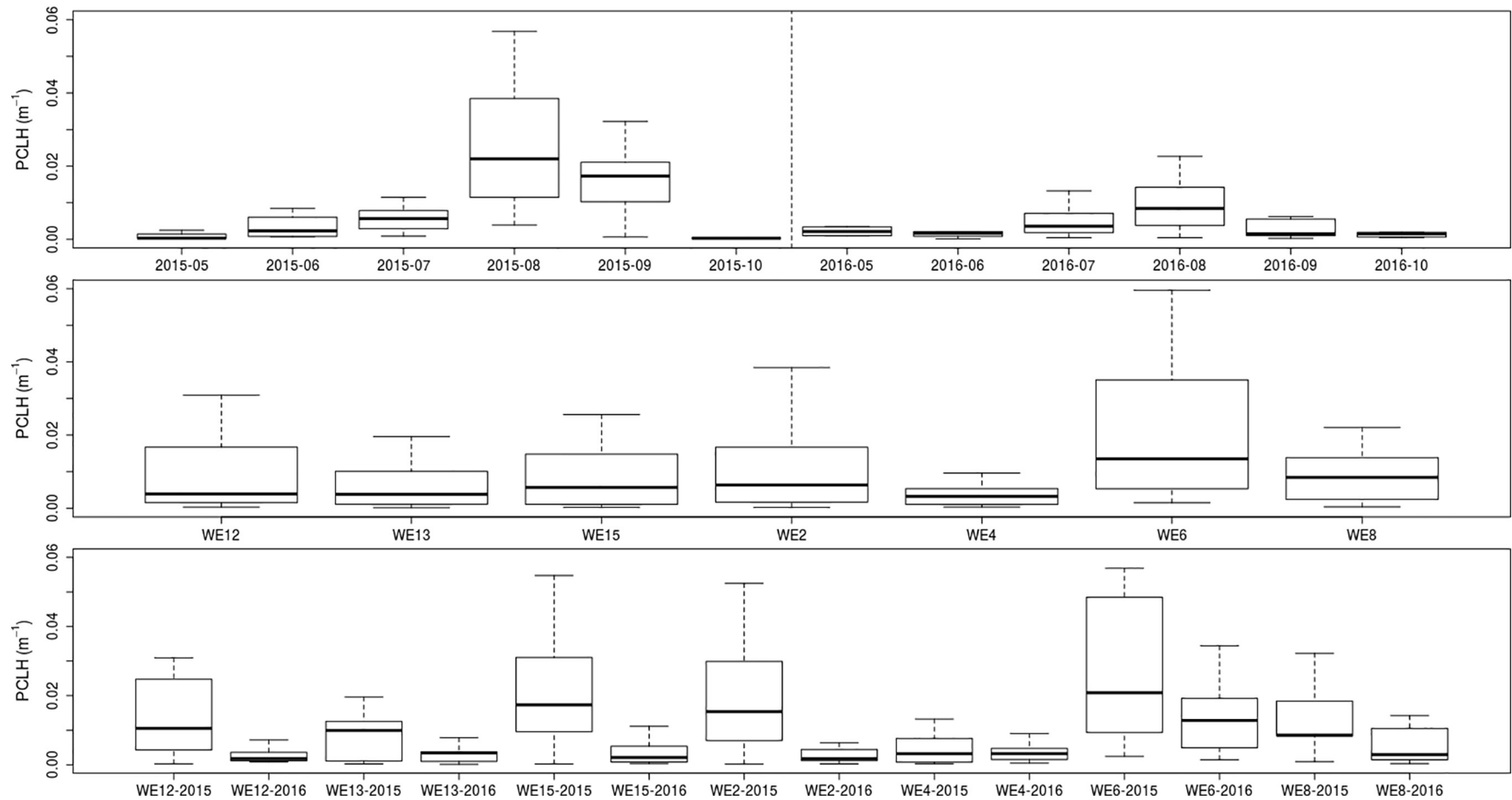
Fig. 7. Spatial and temporal patterns of the particulate absorption phycocyanin line height (PCLH) in western Lake Erie expressed as boxplots where the black horizontal line is the median, the bottom and top of the box are the first and third quartiles respectively, and the horizontal gray lines below and above the box are the minimum and maximum values respectively. Monthly median values for 2015 (left half) and 2016 (right half) are shown in the top panel. Station median values for the combined 2015–2016 dataset are shown in the middle panel. Annual station median values are shown in the bottom panel.
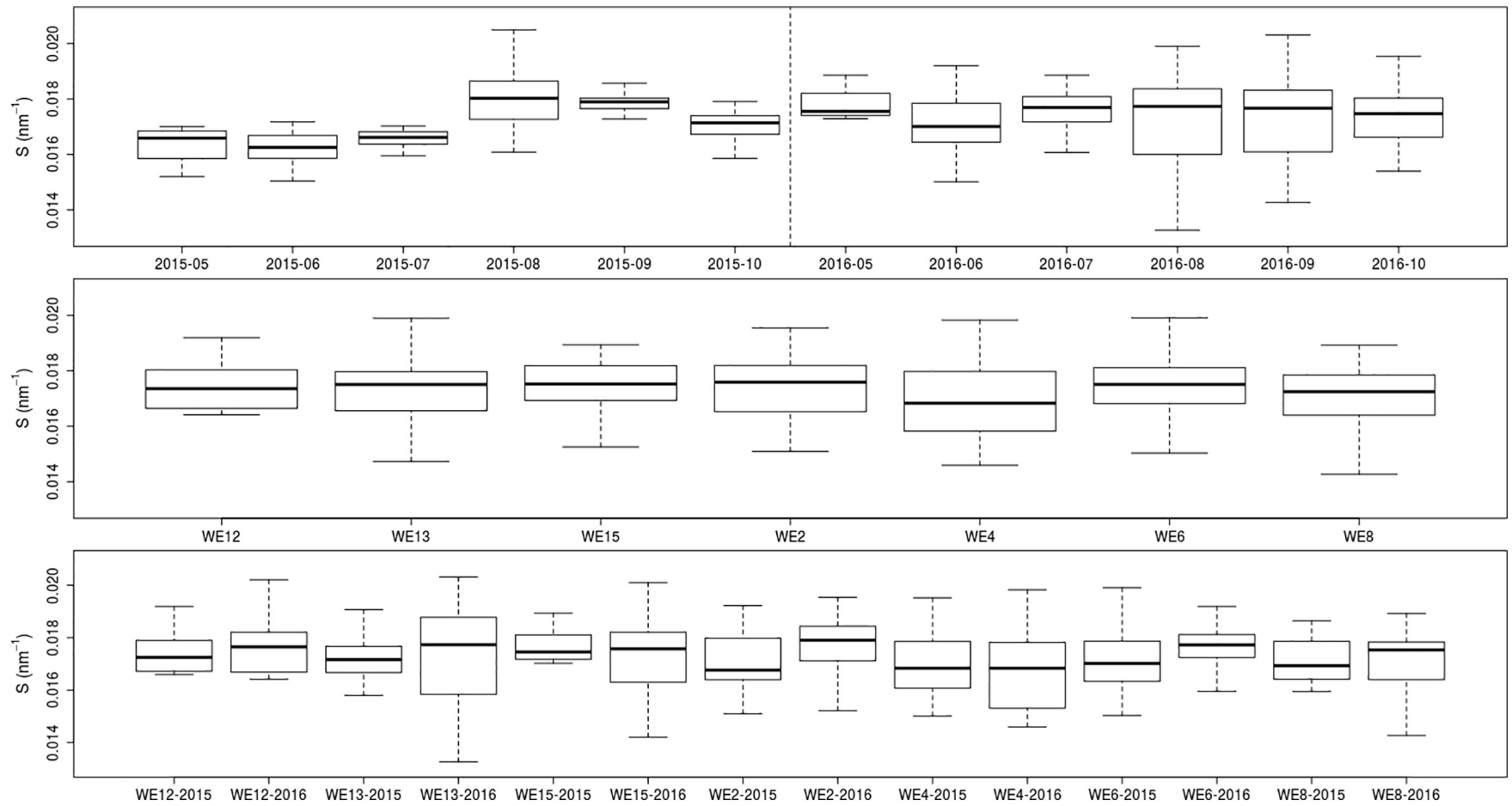
Fig. 8. Spatial and temporal patterns of the CDOM spectral slope, S_{CDOM}, in western Lake Erie expressed as boxplots where the black horizontal line is the median, the bottom and top of the box are the first and third quartiles respectively, and the horizontal gray lines below and above the box are the minimum and maximum values respectively. Monthly median values for 2015 (left half) and 2016 (right half) are shown in the top panel. Station median values for the combined 2015–2016 dataset are shown in the middle panel. Annual station median values are shown in the bottom panel.
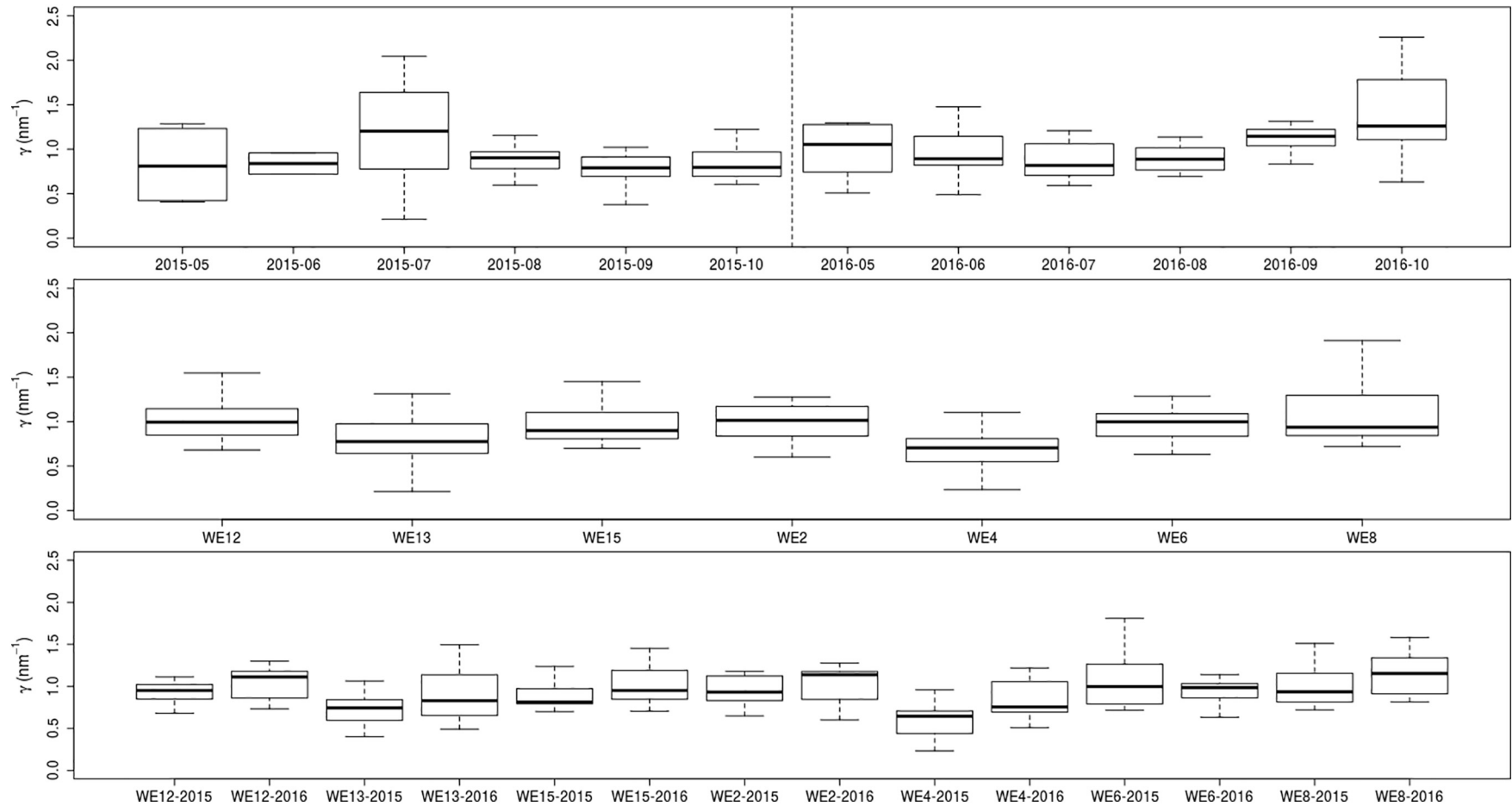
Fig. 9. Spatial and temporal patterns of the particulate beam attenuation spectral slope, γ, in western Lake Erie expressed as boxplots where the black horizontal line is the median, the bottom and top of the box are the first and third quartiles respectively, and the horizontal gray lines below and above the box are the minimum and maximum values respectively. Monthly median values for 2015 (left half) and 2016 (right half) are shown in the top panel. Station median values for the combined 2015–2016 dataset are shown in the middle panel. Annual station median values are shown in the bottom panel.
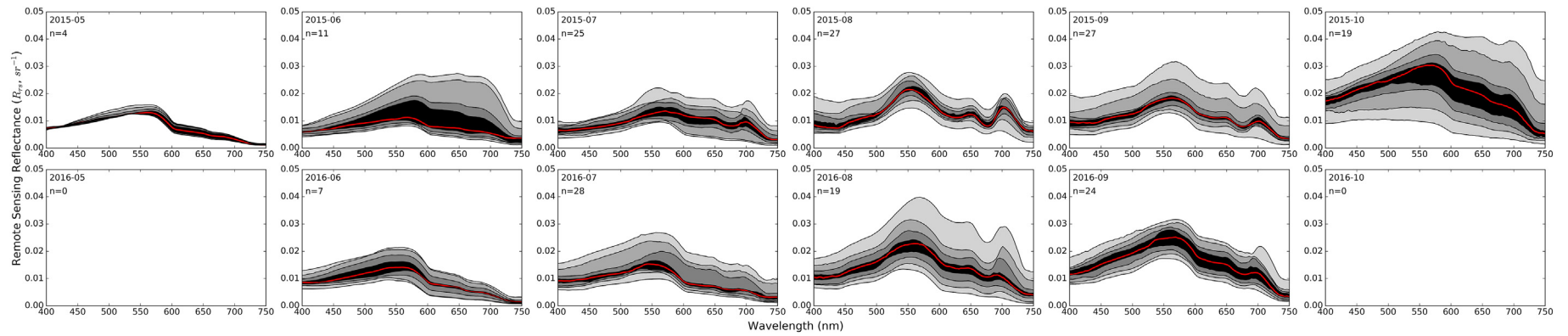
Fig. 10. Temporal patterns in remote sensing reflectance (R_{rs}, sr^{-1}) in western Lake Erie for 2015 (top panels) and 2016 (bottom panels). The monthly mean spectra are displayed as red lines. Variability in monthly spectra are also shown in the gray-black regions around the mean spectra where each color represents a percentage of measured R_{rs} values, following the method described by Hochberg et al. (2003) (light gray = 2.5–97.5%, medium gray = 12.5–87.5%, dark gray = 25–75% and black = 37.5–62.5%). Note, there were no R_{rs} observations for May and October 2016.
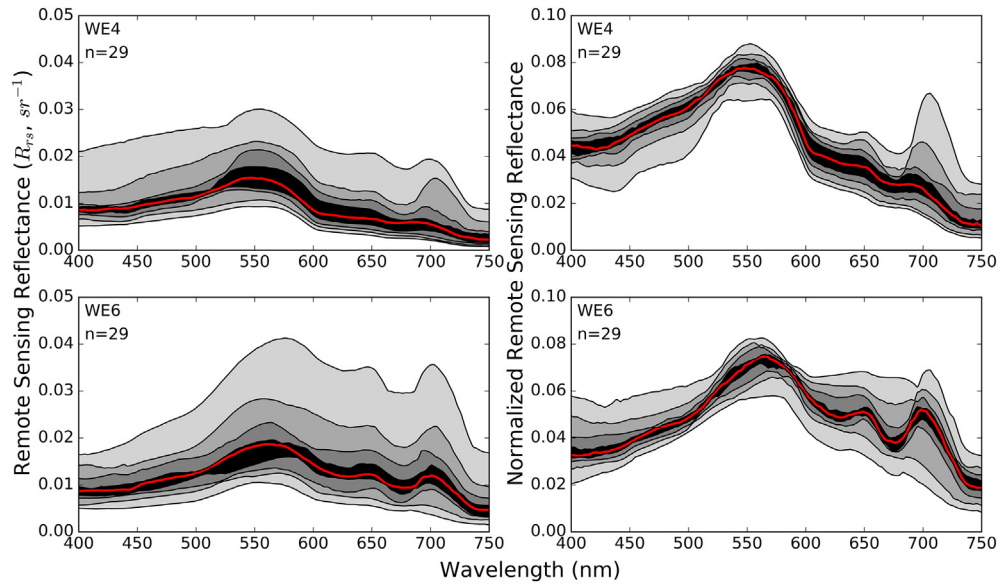
Fig. 11. Study period mean remote sensing reflectance (R_{rs}, sr^{-1}) for stations WE4 (top panels) and WE6 (bottom panels). Absolute R_{rs} (left panels) and normalized R_{rs} (right panels) are shown for both stations. The study period mean spectra are displayed as red lines. Variability in study period spectra are also shown in the gray-black regions around the mean spectra where each color represents a percentage of measured R_{rs} values, following the method described by Hochberg et al. (2003) (light gray = 2.5–97.5%, medium gray = 12.5–87.5%, dark gray = 25–75% and black = 37.5–62.5%).

it is expected that the IOP proxy variability should correlate with changes in R_{rs}. An example of this relationship is shown in Fig. 12 which is a scatterplot between $PCLH_{ap}$ (y-axis) and $PCLH_{Rrs}$ (x-axis). $PCLH_{Rrs}$ was calculated from the measured R_{rs} spectra using the same line height approach and the same wavelengths as the $PCLH_{ap}$ (refer to Methods section). Because the spectral feature of interest (PC

absorption) is a trough in the R_{rs} spectra the $PCLH_{Rrs}$ values are negative as opposed to positive for the $PCLH_{ap}$. In Fig. 12, the $PCLH_{Rrs}$ values were multiplied by -1 in order to express the values as positive numbers. Samples shown on Fig. 12 are binned into two groups where the lab based PC/Chl-a ratio was less than or equal to 0.1 (blue dots) and >0.1 (red dots). These groups represent samples dominated by PC (red
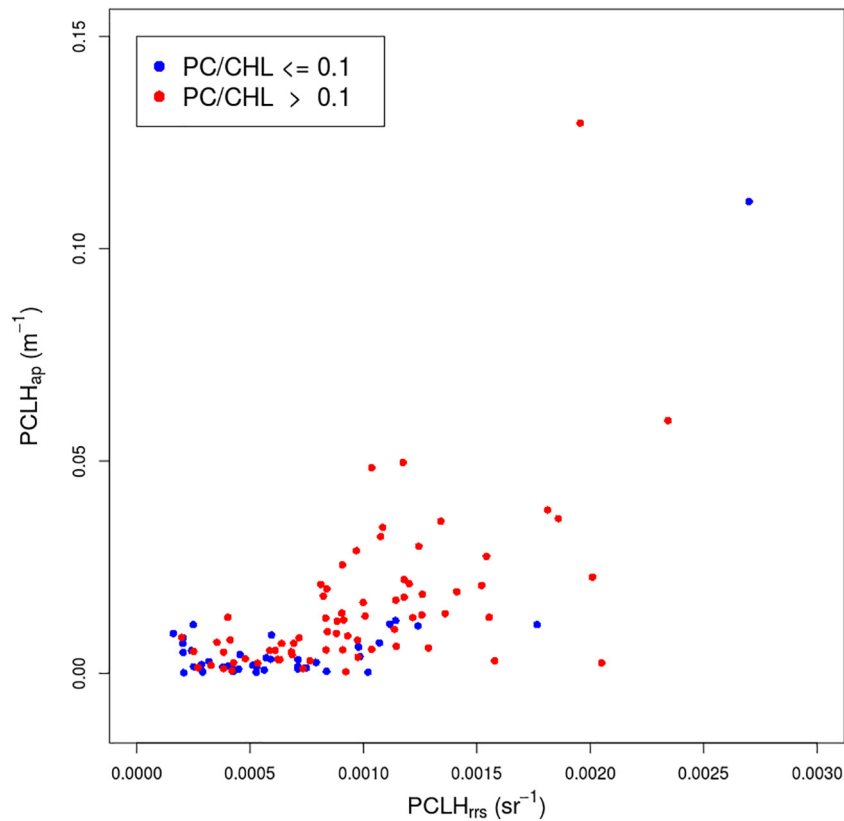

Fig. 12. Comparison between particulate absorption phycocyanin line height ($PCLH_{ap}$) (y-axis) and remote sensing reflectance phycocyanin line height ($PCLH_{Rrs}$) (x-axis). Observations where the phycocyanin to chlorophyll-a ratio (PC/CHL) is low (≤0.1) are shown as blue dots while high PC/CHL ratio (>0.1) observations are displayed as red dots.

dots) and Chl-a (blue dots) respectively. The plot reveals a positive trend between PCLH$_{ap}$ and PCLH$_{Rrs}$ for PCLH$_{Rrs}$ values greater than approximately 0.00075 sr^{-1}. Note that the majority of Chl-a dominated samples (blue dots) result in a very small change in PCLH$_{Rrs}$; however, several samples do result in an increase in PCLH$_{Rrs}$ although less so than those PC dominated samples. Many of the PC dominated samples (red dots) positively correlate with PCLH$_{Rrs}$ however with a high degree of variability. This variability is expected as R$_{rs}$ is controlled by both absorption as well as backscatter, the latter of which is not accounted for in this plot. Never the less, Fig. 12 suggests observed changes in R$_{rs}$ at 620 nm are at least partially explained by changes in particulate absorption, which is highly correlated with increased PC abundance (recall Fig. 6). This result is the basis for remote sensing algorithms aiming to retrieve PC concentration (e.g. Simis et al., 2005).

Discussion

A unique aspect of this study is the documentation of significant temporal IOP variability over the May–October period for two full years (2015–2016). Overall, very limited temporal IOP observations exist in the Great Lakes as a whole and are mostly limited to two samplings from different years (Perkins et al., 2013). Several studies characterizing IOPs in Lake Erie have been limited to cruises spanning several days with station revisits on monthly time scales. Binding et al. (2008) conducted IOP sampling cruises in September 2004 and May, July, and September 2005 with the sampling stations located throughout the western, central, and eastern basins of Lake Erie. O'Donnell et al. (2010) made IOP observations in the western basin of Lake Erie in September 2007 but they only occurred over a two-day period. Because of the limited temporal sampling of these studies, it is likely that only a subset of the range in IOP and optically active constituent variability was quantified. For example, Binding et al. (2008) reported the range of a$_{CDOM}$ at 440 nm as 0.08 to 0.75 m^{-1} while for this study the range was 0.05 to 6.74 m^{-1}, a ~9-fold difference in maximum value, with the highest values occurring in July and August. Similarly, O'Donnell et al. (2010) noted a range in the particulate scattering (b$_p$) spectral slope of −0.28 to −1.0 while for this study the range was from 0.57 to −2.81 indicating vastly different particle size distributions were encountered in each study. Only recently reported are IOP observations (Moore et al., 2017) from the month of August, which represents the dominant cyanoHAB period and many times encapsulates the annual peak bloom extent (Wynne and Stumpf, 2015; Sayers et al., this issue). While Moore et al. (2017) provided a very useful bio-optical characterization of cyanobacteria blooms in WBLE, the study periods were limited to the August period for two years, which limits the ability to evaluate how IOPs vary during bloom initiation and senescence. Moreover, little is known about the variability in IOPs in WBLE between years on short time scales. The near weekly sampling for two full years presented in this study provides the necessary temporal scale to better understand WBLE optical dynamics.

A very interesting component of this study is the documentation of the extreme variability in mean monthly IOPs for 2015 and 2016 in the WBLE. For example, the magnitudes in beam attenuation (c), absorption (a), and scattering (b) for October 2015 (high) and 2016 (low) span the entire range of values for all other months and years combined. It is not unexpected that large variability between October 2015 and 2016 was observed, as this is a period of rapid transition in environmental conditions in Lake Erie. Water temperatures are dropping quickly with increasing precipitation and cloud cover, and sediments are being re-suspended from increased wave action. Moreover, as observed in 2011, very large but short-lived (<7 days) cyanoHAB events can also occur, but these blooms do not occur every year (Michalak et al., 2013). The large IOP variability observed in October indicates the necessity of regular in situ sampling during the algal bloom periods in Lake Erie. This variability also suggests that tight satellite and in situ matchup restrictions (e.g. minimal difference in time between

measurement acquisition and satellite overpass) should be considered in order to ensure valid comparisons are made. It is also generally evident from Fig. 3 that IOP values were higher in 2015 than in 2016, which corresponds with the significantly larger cyanoHAB occurrence in 2015 (Sayers et al., this issue). Annual cyanoHAB events in Lake Erie have been shown to be highly variable from year-to-year partially due to varying spring discharge rates from the Maumee River (Stumpf et al., 2016; Sayers et al., 2016). Sayers et al. also presented a relationship between cyanoHAB extents and the number of sediment re-suspension events that are driven by the regional meteorology (wind speed) and basin morphology (depth). Using these predictors (spring discharge and re-suspension events), 2015 is expected to have experienced larger more sustained cyanoHABs than 2016, which is consistent with the IOP observations presented in Fig. 3.

Maumee River discharge rates are also contributing to temporal variability of IOPs. This is evidenced by the almost 25-fold difference in mean monthly discharge between July 2015 (19,300 ft^3/s) and July 2016 (794 ft^3/s) which corresponds to an approximate 1.5-fold difference in b$_p$ (440), >2-fold difference in a$_{pg}$ (440 nm), and 1.6-fold difference in c$_{pg}$ (400 nm). Because July is often the first month of bloom initiation in WBLE the large variability is not surprising as bloom dynamics often change between years. On the other hand, much smaller differences in IOP magnitude were observed between August 2015 and 2016, yet the IOP values were generally near the highest for all months and years combined. Because August is usually within the mid-point of the annual bloom cycle these results are not surprising and indicate a relatively stable period between years, with little variability due to river discharge (August 2015 = 1567 ft^3/s, August 2016 = 640 ft^3/s) but high IOP values are likely due to persistent cyanoHAB presence. Aggregation of IOPs by month allows for simple comparison and identification of seasonal patterns between years and can help link observations to significant controlling factors. Because these seasonal patterns can change between years due to difference in bloom dynamics and other factors, it is critical to monitor IOPs on at least a monthly scale for the June through October period for every year of interest.

One of the most interesting and unique results from this study is the documentation of seasonal variability in a$_{ph}$*665 over the course of the vegetative season for two years. The range in a$_{ph}$*665 observed in this study was similar to the range reported by Moore et al. (2017) (their Fig. 5b) but less than documented by Binding et al. (2008) which observed an order of magnitude larger maximum value. Mean a$_{ph}$*665 values for 2015 (0.0034 m^2 mg^{-1}) and 2016 (0.0038 m^2 mg^{-1}) were 2-fold smaller than the mean value (0.007 m^2 mg^{-1}) reported by Binding et al. (2008) and appear to be lower than those depicted (their Fig. 5b) in Moore et al. (2017) although no mean values were reported for the 665 nm wavelength. It is important to note that in this study a$_{ph}$*665 was calculated from in situ ac-s measurements of a$_p$ using a line height approach, while the other studies were derived spectrophotometrically using filtered water samples that had been measured for both phytoplankton absorption and non-algal particle absorption. Because of the differences in these two approaches, it is expected that the a$_{ph}$*665 calculated in this study would be smaller than those calculated using lab spectrophotometry. Roesler and Barnard (2013) noted a factor of two lower value using the line height method for samples from the marine environment. Assuming a factor of two difference between the two methods, our study mean a$_{ph}$*665 value would be very close to that reported by Binding et al. (2008). Further investigation into coherence of these two methods is needed to understand how intercomparable their values are moving forward.

A steady decline in median a$_{ph}$*665 values from May through August is evident in both years indicating a steady shift in the phytoplankton community size structure from smaller to larger size populations. The lowering of a$_{ph}$*665 is attributable to the pigment package effect (Bricaud et al., 1995) which is a function of pigment abundance and how pigments are arranged within the cell. Larger cells tend to exhibit

higher degrees of pigment packaging thus lower a_{ph}^* values in general. As pointed out in Moore et al. (2017) some of the observed packaging effect (i.e. lower a_{ph}^* values) may be due in part to the formation of large cyanobacteria colonies which could impart a degree of "packaging" well beyond that observed for individual cyanobacteria cells (Matthews and Bernard, 2013; Zhang et al., 2012). Interestingly, median a_{ph}^*665 in August 2015 were significantly less than those for 2016, likely indicating less abundance of large cyanobacteria colonies in 2016. Similarly, the lowest median a_{ph}^*665 values for 2016 were observed in October suggesting the increased presence of larger sized phytoplankton or formations of large cyanobacteria colonies. The difference in the annual trend of a_{ph}^*665 between 2015 and 2016 suggests a very different algal community/size progression for each year. Other studies reporting values of a_{ph}^*665 (Binding et al., 2008; Moore et al., 2017) do not have the fine scale temporal granularity over the full vegetative season to document these observed transitions, which is critical information for remote sensing bio-optical models that utilize values of a_{ph}^*665 for initial parameterization (Shuchman et al., 2013).

In light of the observed temporal trends in a_{ph}^*665 observations, it was somewhat surprising there were no significant differences in a_{ph}^*665 between stations over the combined two-year study period. Studies that also report a_{ph}^* values for Lake Erie did not document variability at a particular station over long time periods but rather at the basin scale, further confirming the novelty of this dataset. Because a_{ph}^*665 values were consistent for stations over the combined two-year period, it would suggest that the fluctuations in phytoplankton/cyanobacteria assemblages over the season occur uniformly across the area represented by the sampling stations. A possible exception may be for station WE4 where the greatest variability in a_{ph}^*665 was observed. WE4 is located approximately equidistant from the mouths of the Maumee and Detroit Rivers and is situated in 8.5 m deep water. This location appears to be in a transition zone between predominantly Maumee River water and Detroit River water that can switch between the two depending on currents and flows. Moore et al. (2017) documented this transition in optical properties from the Detroit Plume to Maumee Bay water and noted that this frontal boundary is always present but varies in location depending on "climatic factors". This observation is consistent with the increased variability in IOPs at WE4 relative to other stations not in this transition area. Because a_{ph}^*665 tends to vary uniformly for stations over the season (exception for WE4), it may be possible to assume a temporal mean a_{ph}^*665 value for remote sensing model parameterization for waters inclusive of the sampling stations in this study.

This study is the first to document the use of the particulate absorption line height method, using ac-s data, at the PC absorption peak (~620 nm) to track cyanobacteria abundance. Not only was there a strong correlation between individual sample $PCLH_{ap}$ and PC concentration (Fig. 11, Pearson's correlation 0.72), the monthly median $PCLH_{ap}$ values for 2015 and 2016 clearly follow the same patterns identified in the median laboratory extracted PC concentrations (Fig. 2, Pearson's correlation = 0.96) indicating the method is sensitive to varying levels of pigment abundance. The temporal trends in $PCLH_{ap}$ suggest a much more intense cyanoHAB occurrence in 2015 relative to 2016, with both peaking in August. In terms of spatial extent, the cyanoHAB bloom was more intense in 2015 for all stations except WE4, which showed very similar median $PCLH_{ap}$ values between years. The lack of a large median $PCLH_{ap}$ value at WE4 in 2015 suggests the bloom was only periodically occurring at that location and not of particularly high abundance, which agrees with the notion of WE4 being located in a dynamic transition zone between Detroit River and Maumee River waters. These observations are consistent with those reported by Sayers et al. (this issue) that mapped the areal extents of cyanoHAB blooms for 2015 and 2016 using a modified Chl-a retrieval algorithm. It should be acknowledged that the a_p around 620 nm above the estimated a_{NAP} baseline may not be exclusively due to PC. Chl-a exhibits a small absorption peak in the 620 nm range that may also be included in the $PCLH_{ap}$

value which is a possible source of variability when comparing $PCLH_{ap}$ to laboratory derived PC concentrations. The good agreement between $PCLH_{ap}$ and laboratory PC concentrations confirms the utility of using this spectral feature in remote sensing algorithms to estimate PC (Simis et al., 2005) that have been developed for sensors with wavelengths in this region (algorithm review in Mishra et al., 2017).

The CDOM absorption spectral slope, S, values reported in this study were significantly variable over the two-year study period with minimum and maximum values exceeding those previously reported. The CDOM spectral slope has been shown to relate to the molecular weight of the acids (humic and fulvic) comprising the dissolved material. The ratio of humic acids to fulvic acids have been used as a proxy for CDOM composition (e.g. from phytoplankton decomposition or decay of terrestrial material) (Carder et al., 1989; Yacobi et al., 2003). Regardless of the CDOM composition, the spectral slope is a critical component to incorporate in multi-spectral remote sensing bio-optical models (Twardowski et al., 2004). The range of S_{CDOM} values (0.011 to 0.026 nm^{-1}) in this study was twice as large as those reported in Binding et al. (2008) (0.0128 to 0.0197 nm^{-1}) and five-fold greater than observed by Moore et al. (2017). This range is almost identical to that reported by Babin et al. (2003) (0.011 to 0.025 nm^{-1}) for a wide range of coastal European waters. The much greater range in S_{CDOM} values in this study is not surprising given that the maximum value of $a_{CDOM}443$ was ~9 fold greater than reported in Binding et al. (2008) and almost 6 fold more than what Moore et al. (2017) observed. Given the wide ranges of both S_{CDOM} and $a_{CDOM}443$ between the three studies, the mean S_{CDOM} values of each were in relative agreement with Binding et al. (2007) and Moore et al. (2017) reporting 0.0161 and 0.018 nm^{-1}, respectively, while the overall mean for this study was 0.0173 nm^{-1}. Much of the range in S_{CDOM} values was a result of much larger monthly fluctuations in 2016 especially in August and September with much less variability observed in 2015. This would suggest much greater variations in allochthonous and autochthonous sources of CDOM in 2016 relative to 2015, possibly due to differences in river discharge fluctuations or cyanoHAB abundance between years. Binding et al. (2008) suggested that the preferential adsorption of higher molecular weight CDOM on to suspended mineral particles, leaving only the lower weight fraction free in the water, may alter the bulk absorption properties one may expect to observe, which may well be occurring in these measurements also altering observed patterns.

This study also documents the first reported values of the particulate beam attenuation (c_p) spectral slope, γ, in the Great Lakes. To first order the c_p spectral slope has been shown to relate to the power law slope of the particle size distribution (PSD) both theoretically (Boss et al., 2001) and experimentally (Slade and Boss, 2015), potentially providing information into phytoplankton community structure and sediment transport. The observed range of values of γ in this study was more than two-fold larger than observed in coastal ocean waters (Slade and Boss, 2015) and the bottom boundary layer in the mid-Atlantic Bight (Boss et al., 2001). The large variability in γ suggests highly variable PSDs throughout the two-year period in western Lake Erie with largest fluctuations occurring in July 2015 corresponding to extremely high mean discharge (19,300 ft^3/s compared with long term July mean discharge 2850 ft^3/s) from the Maumee River. August and September for both years exhibited the most consistent γ values suggesting very similar PSDs during the dominant cyanoHAB period while experiencing relatively low discharge rates (<1600 ft^3/s). There was little spatial difference in γ values with only WE4 exhibiting significantly lower values than all other stations. The lower γ values would suggest the presence of a PSD with relatively larger particles likely in the form of large diatoms or other microplankton and less occurrence of small particles consistent with inorganic sediment particles either re-suspended or injected from the river. It should be noted that the acceptance angle (0.93°) on the beam attenuation chamber optic of the ac-s can act as a particle size "filter" for particles larger than 50 μm (Boss et al., 2009; Slade and Boss, 2015). Additionally, the relationship of γ to the PSD slope assumes the PSD slope follows the

form of a negative power law as a function of particle diameter (Bader, 1970), which may not be true in many environments including complex freshwater systems. Boss et al. (2001) also note the presence of strongly absorbing particles may limit the robustness of the relationships between γ and PSD due to anomalous dispersion. Further research into the relationship between γ and PSDs in the Great Lakes, and specifically Lake Erie, is needed to understand these dynamics.

In light of the observed spatial and temporal variability in IOPs and optical proxies in western Lake Erie, uncertainties in remote sensing algorithm retrievals that use fixed model parameterizations need to be evaluated spatially and temporally. Bio-optical remote sensing algorithms rely on knowing some information about the underlying IOPs of the water being sensed (Werdell et al., 2018). Previous investigators have formulated retrieval algorithm frameworks that make assumptions regarding the underlying IOPs, usually from a set of in situ measurements or from reported literature. For example, Binding et al. (2012) proposed an approach to simultaneously retrieve concentrations of minerogenic suspended particulate matter (MSPM) and Chl-a using the red and near-infrared bands of the MODIS Aqua sensor. The Binding et al. (2012) algorithm relates the satellite-observed water leaving radiance at 667 and 748 nm to the water volume absorption and backscatter coefficients using mean mass specific absorption and backscattering coefficients for phytoplankton and non-algal particles (a_{ph}^* and a_{NAP}^*). Through these assumptions, concentrations of MSPM and Chl-a can be estimated. Similarly, Simis et al. (2005) proposed a bio-optical algorithm to retrieve PC concentration through the estimation of PC absorption (a_{pc}) at 620 nm. The algorithm related the ratio of reflectance at 709 and 620 nm to a model for PC absorption and then to PC concentration using an assumed a_{pc}^* value. Finally, Shuchman et al. (2013) reported a bio-optical inversion model to retrieve concentrations of the primary optically active constituents (OACs) Chl-a, CDOM absorption, and fixed suspended solids (FSS) from multi-spectral MODIS imagery. The model relates concentrations of the OACs to observed reflectance values using assumed values for a_{ph}^*, S_{CDOM}, and a_{NAP}^* to minimize the difference between measured and modeled reflectance at all MODIS bands.

Though each of these model frameworks retrieves different water parameters, they all rely on parameterization of specific IOPs, which have been shown in this study to vary in time and space. Variable model parameterization may yield lower uncertainties in model retrievals when deployed throughout the ice-free period. For example, the a_{ph}^*665 value used in the Binding et al. (2012) model is 0.025 m^2 mg^{-1}, which is approximately 1.6 times greater than the largest a_{ph}^*665 value observed in this study (0.015 m^2 mg^{-1}) and almost seven times greater than the study mean value (0.004 m^2 mg^{-1}). Even after transforming the a_{ph}^*665 values in this study to values comparable in magnitude with Binding et al. (2012) (i.e. multiplication by a factor of two, Roesler and Barnard (2013)), the transformed study mean value (0.008 m^2 mg^{-1}) is still a factor of three lower than the 0.025 m^2 mg^{-1} value used in Binding et al. (2012). It is possible that an adaptive parameterization of a_{ph}^*665 in the Binding et al. (2012) model over the observed range of values could provide more accurate retrievals of both Chl-a and FSS in both cyanobacteria and non-cyanobacteria conditions. Additionally, Simis et al. (2005) acknowledge the high degree of variability of a_{pc}^*620 in response to changing environmental conditions and suggest that if specific knowledge of the variability in a_{pc}^*620 is known or can be estimated for a particular environment of interest, more accurate retrievals should be attainable. Similar to the other two model frameworks, the Shuchman et al. (2013) approach assumes a S_{CDOM} value of 0.016 nm^{-1} which is similar to that reported in Binding et al. (2008) (0.0161 nm^{-1}) but lower than the mean values reported by Moore et al. (2017) (0.018 nm^{-1}) and in this study (0.0173 nm^{-1}). In addition, the large range of S_{CDOM} observed in this study suggests that the model default parameterization may be significantly different from the actual value for a given date and location depending on environmental factors. Further investigation into how remote sensing algorithm accuracy and uncertainty varies as a function of different parameterizations is warranted and should ultimately lead to more accurate water quality products.

Conclusion

Presented in this study is a unique IOP data set for western Lake Erie that spans the vegetative season over two full years. Weekly observations at the same locations over a long period (six months) allows insights into the natural variability of IOPs as a function of changing algal communities, river discharge fluctuations, and various other environmental forcing functions. Spatial variations in IOPs were identified and related to the proximity of a station to significant river discharge plumes. Significant variability in IOPs shape and magnitude were observed on weekly and monthly scales suggesting in situ measurements should be collected at least monthly in western Lake Erie to adequately track the significant variability.

This study documented significant shifts in the mass specific phytoplankton absorption coefficient, a_{ph}^*665, from the May through August period associated with the development of significant colonial cyanobacteria blooms. Differences in annual progression and magnitude of a_{ph}^*665 between 2015 and 2016 suggests the relative intensity of the annual bloom is a dominant factor controlling the distribution of a_{ph}^*665 values in western Lake Erie from year to year. Further measurements of a_{ph}^*665 at short time scales over the full vegetative season are needed to fully understand how shifts in algal communities vary as a function of cyanoHAB extent and intensity.

Other IOP variables displayed significant variability over the two-year dataset with the $PCLH_{ap}$ exhibiting a seasonal trend in association with the cyanoHAB progression, while S_{CDOM} and the c_p spectral slope exhibited variability more associated with environmental forcing functions. Fully understanding the complex IOP variability associated with unpredictable driving factors, such as increased discharge rates from high precipitation events and wind driven sediment re-suspension, will require further investigation and targeted sampling efforts to capture the full range of optical variability over these relatively short-lived events.

Finally, remote sensing water quality retrieval algorithms that assume a single IOP parameterization can yield meaningful results on the average (e.g. annually); however, significant errors may be present for time periods and locations where the model optical parameters are significantly different than the actual properties. The IOP dataset presented in this study has shed some light on how these properties change over the course of a season and between years, and may be useful in advancing the applicability and robustness of remote sensing methods to retrieve valuable water quality information in western Lake Erie.

Acknowledgements

References

American Public Health Association, A.P.H.A., 1998. Standard methods for the examination of water and wastewater.
Babin, M., Stramski, D., Ferrari, G.M., Claustre, H., Bricaud, A., Obolensky, G., Hoeffner, N., 2003. Variations in the light absorption coefficients of phytoplankton, nonalgal particles, and dissolved organic matter in coastal waters around Europe. J. Geophys. Res. Oceans (C7), 108.

Bader, H., 1970. The hyperbolic distribution of particle sizes. J. Geophys. Res. 75 (15), 2822–2830.

Bailey, S.W., Werdell, P.J., 2006. A multi-sensor approach for the on-orbit validation of ocean color satellite data products. Remote Sens. Environ. 102 (1–2), 12–23.

Barbiero, R.P., Lesht, B.M., Hinchey, E.K., Nettesheim, T.G., 2018. A brief history of the US EPA Great Lakes National Program Office's water quality survey. J. Great Lakes Res. 44 (4), 539–546.

Becker, R.H., Sultan, M.I., Boyer, G.L., Twiss, M.R., Konopko, E., 2009. Mapping cyanobacterial blooms in the Great Lakes using MODIS. J. Great Lakes Res. 35 (3), 447–453.

Binding, C.E., Jerome, J.H., Bukata, R.P., Booty, W.G., 2007. Trends in water clarity of the lower Great Lakes from remotely sensed aquatic color. J. Great Lakes Res. 33 (4), 828–841.

Binding, C.E., Jerome, J.H., Bukata, R.P., Booty, W.G., 2008. Spectral absorption properties of dissolved and particulate matter in Lake Erie. Remote Sens. Environ. 112 (4), 1702–1711.

Binding, C.E., Greenberg, T.A., Bukata, R.P., 2012. An analysis of MODIS-derived algal and mineral turbidity in Lake Erie. J. Great Lakes Res. 38 (1), 107–116.

Binding, C.E., Greenberg, T.A., Watson, S.B., Rastin, S., Gould, J., 2015. Long term water clarity changes in North America's Great Lakes from multi-sensor satellite observations. Limnol. Oceanogr. 60 (6), 1976–1995.

Boss, E., Slade, W.H., Behrenfeld, M., Dall'Olmo, G., 2009. Acceptance angle effects on the beam attenuation in the ocean. Opt. Express 17 (3), 1535–1550.

Boss, E., Twardowski, M.S., Herring, S., 2001. Shape of the particulate beam attenuation spectrum and its inversion to obtain the shape of the particulate size distribution. Appl. Opt. 40 (27), 4885–4893.

Bosse, K.R., Sayers, M.J., Shuchman, R.A., Fahnenstiel, G.L., Ruberg, S.A., Fanslow, D.L., Stuart, D.G., Johengen, T.H., Burtner, A.M., 2019. Spatial-temporal variability of in situ cyanobacteria vertical structure in Western Lake Erie: Implications for remote sensing observations. J. Great Lakes Res.

Bricaud, A., Babin, M., Morel, A., Claustre, H., 1995. Variability in the chlorophyll-specific absorption coefficients of natural phytoplankton: analysis and parameterization. J. Geophys. Res. Oceans 100 (C7), 13321–13332.

Bricaud, A., Claustre, H., Ras, J., Oubelkheir, K., 2004. Natural variability of phytoplanktonic absorption in oceanic waters: Influence of the size structure of algal populations. J. Geophys. Res. Oceans 109 (C11).

Bridgeman, T.B., Chaffin, J.D., Filbrun, J.E., 2013. A novel method for tracking western Lake Erie Microcystis blooms, 2002–2011. J. Great Lakes Res. 39 (1), 83–89.

Carder, K.L., Steward, R.G., Harvey, G.R., Ortner, P.B., 1989. Marine humic and fulvic acids: their effects on remote sensing of ocean chlorophyll. Limnol. Oceanogr. 34 (1), 68–81.

Ciotti, A.M., Lewis, M.R., Cullen, J.J., 2002. Assessment of the relationships between dominant cell size in natural phytoplankton communities and the spectral shape of the absorption coefficient. Limnol. Oceanogr. 47 (2), 404–417.

Conroy, J.D., Edwards, W.J., Pontius, R.A., Kane, D.D., Zhang, H., Shea, J.F., Richey, J.N., Culver, D.A., 2005. Soluble nitrogen and phosphorus excretion of exotic freshwater mussels (Dreissena spp.): potential impacts for nutrient remineralisation in western Lake Erie. Freshw. Biol. 50 (7), 1146–1162.

Effler, S.W., Perkins, M., Peng, F., Strait, C., Weidemann, A.D., Auer, M.T., 2010. Light-absorbing components in Lake Superior. J. Great Lakes Res. 36 (4), 656–665.

Gordon, H.R., McCluney, W.R., 1975. . Estimation of the depth of sunlight penetration in the sea for remote sensing. Appl. Opt. 14 (2), 413–416.

Ho, J.C., Michalak, A.M., 2017. Phytoplankton blooms in Lake Erie impacted by both long-term and springtime phosphorus loading. J. Great Lakes Res. 43 (3), 221–228.

Ho, J.C., Stumpf, R.P., Bridgeman, T.B., Michalak, A.M., 2017. Using Landsat to extend the historical record of lacustrine phytoplankton blooms: a Lake Erie case study. Remote Sens. Environ. 191, 273–285.

Hochberg, E.J., Atkinson, M.J., Andréfouët, S., 2003. Spectral reflectance of coral reef bottom-types worldwide and implications for coral reef remote sensing. Remote Sens. Environ. 85 (2), 159–173.

Horváth, H., Kovács, A.W., Riddick, C., Présing, M., 2013. Extraction methods for phycocyanin determination in freshwater filamentous cyanobacteria and their application in a shallow lake. Eur. J. Phycol. 48 (3), 278–286.

IOCCG, 2014. Phytoplankton functional types from space. Reports of the International Ocean-Colour Coordinating Group, No. 15, p. 156.

Jones, E., Oliphant, T., Peterson, P., 2001. SciPy: open source scientific tools for Python. Online; accessed 2015-05-11. URL http://www.scipy.org.

Kane, D.D., Conroy, J.D., Richards, R.P., Baker, D.B., Culver, D.A., 2014. Re-eutrophication of Lake Erie: correlations between tributary nutrient loads and phytoplankton biomass. J. Great Lakes Res. 40 (3), 496–501.

Lesht, B.M., Barbiero, R.P., Warren, G.J., 2013. A band-ratio algorithm for retrieving open-lake chlorophyll values from satellite observations of the Great Lakes. J. Great Lakes Res. 39 (1), 138–152.

Mann, H.B., Whitney, D.R., 1947. On a test of whether one of two random variables is stochastically larger than the other. Ann. Math. Stat. 50–60.

Matthews, M.W., Bernard, S., 2013. Characterizing the absorption properties for remote sensing of three small optically-diverse South African reservoirs. Remote Sens. 5 (9), 4370–4404.

Michalak, A.M., Anderson, E.J., Beletsky, D., Boland, S., Bosch, N.S., Bridgeman, T.B., Chaffin, J.D., Cho, K., Confesor, R., Daloğlu, I., DePinto, J.V., 2013. Record-setting algal bloom in Lake Erie caused by agricultural and meteorological trends consistent with expected future conditions. Proc. Natl. Acad. Sci. 110 (16), 6448–6452.

Mishra, D.R., Ogashawara, I., Gitelson, A.A. (Eds.), 2017. Bio-optical Modeling and Remote Sensing of Inland Waters. Elsevier.

Mobley, C.D., 1999. Estimation of the remote-sensing reflectance from above-surface measurements. Appl. Opt. 38 (36), 7442–7455.

Moore, T.S., Dowell, M.D., Bradt, S., Verdu, A.R., 2014. An optical water type framework for selecting and blending retrievals from bio-optical algorithms in lakes and coastal waters. Remote Sens. Environ. 143, 97–111.

Moore, T.S., Mouw, C.B., Sullivan, J.M., Twardowski, M.S., Burtner, A.M., Ciochetto, A.B., McFarland, M.N., Nayak, A.R., Paladino, D., Stockley, N.D., Johengen, T.H., 2017. Bio-optical properties of cyanobacteria blooms in western Lake Erie. Front. Mar. Sci. 4, 300.

Morel, A., Prieur, L., 1977. Analysis of variations in ocean color. Limnol. Oceanogr. 22 (4), 709–722.

Mouw, C.B., Hardman-Mountford, N.J., Alvain, S., Bracher, A., Brewin, R.J., Bricaud, A., Ciotti, A.M., Devred, E., Fujiwara, A., Hirata, T., Hirawake, T., 2017. A consumer's guide to satellite remote sensing of multiple phytoplankton groups in the global ocean. Front. Mar. Sci. 4, 41.

Mueller, J.L., 2003. In-water radiometric profile measurements and data analysis protocols. Ocean optics protocols for satellite ocean color sensor validation. Revision 4, 7–20.

O'Donnell, D.M., Effler, S.W., Strait, C.M., Leshkevich, G.A., 2010. Optical characterizations and pursuit of optical closure for the western basin of Lake Erie through in situ measurements. J. Great Lakes Res. 36 (4), 736–746.

Perkins, M., Effler, S.W., Peng, F., O'Donnell, D.M., Strait, C., 2013. Light-absorbing components in the Great Lakes. J. Great Lakes Res. 39, 123–136.

Roesler, C.S., Barnard, A.H., 2013. Optical proxy for phytoplankton biomass in the absence of photophysiology: rethinking the absorption line height. Methods in Oceanog. 7, 79–94.

Röttgers, R., McKee, D., Woźniak, S.B., 2013. Evaluation of scatter corrections for ac-9 absorption measurements in coastal waters. Methods in Oceanography 7, 21–39.

Roy, S., Llewellyn, C.A., Egeland, E.S., Johnsen, G. (Eds.), 2011. Phytoplankton pigments: characterization, chemotaxonomy and applications in oceanography. Cambridge University Press.

Savitzky, A., Golay, M.J., 1964. Smoothing and differentiation of data by simplified least squares procedures. Anal. Chem. 36 (8), 1627–1639.

Sayers, M., Fahnenstiel, G.L., Shuchman, R.A., Whitley, M., 2016. Cyanobacteria blooms in three eutrophic basins of the Great Lakes: a comparative analysis using satellite remote sensing. Int. J. Remote Sens. 37 (17), 4148–4171.

Sayers, M., Grimm, A.G., Shuchman, R.A., Bosse, K.R., Fahnenstiel, G.L., Ruberg, S.A., Leshkevich, G.A., 2019. Satellite monitoring of harmful algal blooms in the western basin of Lake Erie: a 20-year time-series. J. Great Lakes Res. (this issue).

Scientific, Sea-Bird, 2011. AC Meter Protocol Document, Revision Q.

Sea-Bird Scientific, 2017. Prosoft 7.7 Software User Manual

Shuchman, R.A., Leshkevich, G., Sayers, M.J., Johengen, T.H., Brooks, C.N., Pozdnyakov, D., 2013. An algorithm to retrieve chlorophyll, dissolved organic carbon, and suspended minerals from Great Lakes satellite data. J. Great Lakes Res. 39, 14–33.

Simis, S.G., Peters, S.W., Gons, H.J., 2005. Remote sensing of the cyanobacterial pigment phycocyanin in turbid inland water. Limnol. Oceanogr. 50 (1), 237–245.

Slade, W.H., Boss, E., 2015. Spectral attenuation and backscattering as indicators of average particle size. Appl. Opt. 54 (24), 7264–7277.

Smith, D.R., King, K.W., Williams, M.R., 2015. What is causing the harmful algal blooms in Lake Erie? J. Soil Water Conserv. 70 (2), 27A–29A.

Speziale, B.J., Schreiner, S.P., Giammatteo, P.A., Schindler, J.E., 1984. Comparison of N, N-dimethylformamide, dimethyl sulfoxide, and acetone for extraction of phytoplankton chlorophyll. Can. J. Fish. Aquat. Sci. 41 (10), 1519–1522.

Stumpf, R.P., Wynne, T.T., Baker, D.B., Fahnenstiel, G.L., 2012. Interannual variability of cyanobacterial blooms in Lake Erie. PLoS One 7 (8), e42444.

Stumpf, R.P., Johnson, L.T., Wynne, T.T., Baker, D.B., 2016. Forecasting annual cyanobacterial bloom biomass to inform management decisions in Lake Erie. J. Great Lakes Res. 42 (6), 1174–1183.

Sullivan, J.M., Twardowski, M.S., Zaneveld, J.R.V., Moore, C.M., Barnard, A.H., Donaghay, P.L., Rhoades, B., 2006. Hyperspectral temperature and salt dependencies of absorption by water and heavy water in the 400–750 nm spectral range. Appl. Opt. 45 (21), 5294–5309.

Twardowski, M.S., Boss, E., Sullivan, J.M., Donaghay, P.L., 2004. Modeling the spectral shape of absorption by chromophoric dissolved organic matter. Mar. Chem. 89 (1–4), 69–88.

Vanderploeg, H.A., Liebig, J.R., Carmichael, W.W., Agy, M.A., Johengen, T.H., Fahnenstiel, G.L., Nalepa, T.F., 2001. Zebra mussel (Dreissena polymorpha) selective filtration promoted toxic Microcystis blooms in Saginaw Bay (Lake Huron) and Lake Erie. Can. J. Fish. Aquat. Sci. 58 (6), 1208–1221.

Vincent, R.K., Qin, X., McKay, R.M.L., Miner, J., Czajkowski, K., Savino, J., Bridgeman, T., 2004. Phycocyanin detection from LANDSAT TM data for mapping cyanobacterial blooms in Lake Erie. Remote Sens. Environ. 89 (3), 381–392.

Wei, J., Lee, Z., Shang, S., 2016. A system to measure the data quality of spectral remote-sensing reflectance of aquatic environments. J. Geophys. Res. Oceans 121 (11), 8189–8207.

Werdell, P.J., Bailey, S.W., 2005. An improved in-situ bio-optical data set for ocean color algorithm development and satellite data product validation. Remote Sens. Environ. 98 (1), 122–140.

Werdell, P.J., McKinna, L.I., Boss, E., Ackleson, S.G., Craig, S.E., Gregg, W.W., Lee, Z., Maritorena, S., Roesler, C.S., Rousseaux, C.S., Stramski, D., 2018. An overview of approaches and challenges for retrieving marine inherent optical properties from ocean color remote sensing. Prog. Oceanogr. 160, 186–212.

Wynne, T.T., Stumpf, R.P., 2015. Spatial and temporal patterns in the seasonal distribution of toxic cyanobacteria in western Lake Erie from 2002–2014. Toxins 7 (5), 1649–1663.

Wynne, T.T., Stumpf, R.P., Tomlinson, M.C., Warner, R.A., Tester, P.A., Dyble, J., Fahnenstiel, G.L., 2008. Relating spectral shape to cyanobacterial blooms in the Laurentian Great Lakes. Int. J. Remote Sens. 29 (12), 3665–3672.

Yacobi, Y.Z., Alberts, J.J., Takacs, M., McElvaine, M.L., 2003. Absorption Spectroscopy of Colored Dissolved Organic Carbon in Georgia (USA) Rivers: The Impact of Molecular Size Distribution.

Zhang, Y., Yin, Y., Wang, M., Liu, X., 2012. Effect of phytoplankton community composition and cell size on absorption properties in eutrophic shallow lakes: field and experimental evidence. Opt. Express 20 (11), 11882–11898.